

To appear in The Astrophysical Journal

**Multiwavelength Study of the Starburst Galaxy NGC 7714.
II. The Balance between Young, Intermediate Age and Old Stars**

Ariane Lançon

*Obs. de Strasbourg (UMR 7550), 11 rue de l'Université, 67000 Strasbourg, France
lancon@astro.u-strasbg.fr*

Jeffrey D. Goldader

*Univ. of Pennsylvania, Dept. of Phys. & Astron., 209 S. 33rd St., Philadelphia, PA 19104
jdgoldad@dept.physics.upenn.edu*

Claus Leitherer

*Space Telescope Science Institute¹, 3700 San Martin Drive, Baltimore, MD 21218
leitherer@stsci.edu*

and

Rosa M. González Delgado

*Instituto de Astrofísica de Andalucía (CSIC), Apdo. 3004, 18080 Granada, Spain
rosa@iaa.es*

ABSTRACT

We combine existing multiwavelength data (including an HST/GHRS UV spectrum and a ground based optical spectrum) with unpublished HST/WFPC2 images, near-IR photometry and K band spectroscopy. We use these data to constrain the young, the intermediate age and the old stellar populations in the central regions of the starburst galaxy NGC 7714.

In a previous paper (González Delgado et al. 1999), the stellar features in the HST/GHRS ultraviolet (UV) spectrum and the optical emission lines were used to identify a ~ 5 Myr old, very little reddened stellar population as the main source of UV light in the central ~ 330 pc. The optical data indicated the existence of an older population. The nature of the latter is investigated here. Stellar absorption features in the optical and the near-IR are used to partly break the strong degeneracy between the

¹Operated by AURA, Inc., under NASA contract NAS5-26555

effects of ageing and those of the inhomogeneous dust distribution on the UV–optical–IR colors. Consistency with far-IR, X-ray and radio data is also addressed. The successful models have essential features in common. We find that the young burst responsible for the UV light represents only a small part of an extended episode of enhanced star formation, initiated a few 10^8 yrs ago. The star formation rate is likely to have varied on this timescale, averaging about $1 M_{\odot} \text{ yr}^{-1}$. The mass of young and intermediate age stars thus formed equals at least 10% of the mass locked in pre-existing stars of the underlying spiral galaxy nucleus, and fractions around 25% are favored. The spectrophotometric star formation timescale is long compared to the ~ 110 Myr elapsed since closest contact with the neighboring NGC 7715, according to the dynamical models of Smith & Wallin (1992). The initial trigger of the starburst thus remains elusive.

NGC 7714 owes its brightness in the UV to a few low extinction lines of sight towards young stars. Our results based on the integrated spectrophotometry of the central ~ 330 pc are supported by high resolution images of this area. The different extinction values obtained when different spectral indicators are used result naturally from the coexistence of populations with various ages and obscurations. The near-IR continuum image looks smoothest, as a consequence of lower sensitivity to extinction and of a larger contribution of old stars.

We compare the nuclear properties of NGC 7714 with results from studies in larger apertures. We emphasize that the global properties of starburst galaxies are the result of the averaging over many lines of sight with very diverse properties in terms of obscuration and stellar ages. The overall picture is strongly reminiscent of the other nearby “proto-typical” starburst, M 82.

Subject headings: dust, extinction—galaxies: individual (NGC 7714)—galaxies: ISM—galaxies: starburst—galaxies: stellar content

1. Introduction

A burst of star formation in a galaxy affects the galaxy’s energy output across the entire electromagnetic spectrum. Supernovae emit X-rays; the continua of hot massive stars are strong in the ultraviolet (UV); gaseous recombination lines dominate the optical spectra; cool stars are strong emitters in the near-infrared (near-IR); dust heated by the absorption of energetic photons can produce strong far-IR emission; and synchrotron radiation from electrons accelerated by supernova remnants is important at radio wavelengths. Yet, the physical manifestations of a starburst depend on its age. Old starbursts (\gtrsim tens of Myr), where the majority of the massive stars have evolved off the main sequence or already died, will have relatively little UV emission, though red supergiants (RSG), red giants, or asymptotic giant branch (AGB) stars could cause them to be quite bright in the near-IR. On the other hand, a very young starburst (\lesssim few Myr) will have strong UV emission, yet relatively weak IR emission, since IR luminous stars have not yet formed. For a recent review

see, e.g., Leitherer (2000).

The effects of starbursts have been studied in great detail for large samples at individual wavelengths. Multiwavelength studies of starbursts at galaxy-scale resolution were done by, e.g., Calzetti (1997), Schmitt et al. (1997), and Mas-Hesse & Kunth (1999). But few studies have attempted a panchromatic approach that combines high spatial resolution with both photometric and spectroscopic information, focussing on one object, thereby studying star formation in an individual galaxy at the greatest possible detail.

One motivation for programs aiming at very high spatial resolution is disentangling the complex effects of reddening by dust (with various extinction geometries) from “secular” age-induced reddening as stellar populations age. For all dusty starbursts, the reddening correction is an essential step in the determination of the total amount of star formation. The conversion of reddening measurements into attenuation factors is non trivial, even for “simple” stellar populations (Witt & Gordon 2000). For instance, it has often been suggested that emission lines are affected by more extinction than stellar continuum emission (e.g. Calzetti et al. 1994). Only the detailed analysis of spectrophotometric properties in the light of high resolution imaging data will allow us to understand what is really happening and to gain confidence in results for more distant objects, for which only integrated spectrophotometry is available.

We have chosen to study the prototypical starburst galaxy NGC 7714 (Weedman et al. 1981). This spiral galaxy at a distance of 37.3 Mpc (for $H_0 = 75 \text{ km s}^{-1} \text{ Mpc}^{-1}$ and $cz = 2798 \text{ km s}^{-1}$) is interacting with its smaller neighbor NGC 7715 (see references in González Delgado et al. 1999, hereafter Paper I). The inclination of NGC 7714 is $\sim 45^\circ$, allowing a fairly clear view of the inner few hundred pc ($1''$ is equivalent to 189 pc at 37.3 Mpc), where the strongest star formation is occurring. Though luminous in the IR ($L_{\text{IR}} = 3 \times 10^{10} L_\odot$; see Paper I), NGC 7714 is a strong UV source as well. Together, these facts are evidence that the mean dust obscuration is not too severe. This gave us hope that we could use data from the spacecraft UV to model directly the UV continuum of the hot, young stars, providing powerful constraints on the starburst age. This was the major topic of Paper I.

The *global* properties of NGC 7714 were studied previously by Calzetti (1997), who analyzed large-aperture ($10'' \times 20''$, $1.9 \text{ kpc} \times 3.8 \text{ kpc}$) multiwavelength photometry and spectroscopy similar to the data in our study. However, we concentrate on the inner few hundred pc of the nucleus, where the most intense star formation is occurring.

As part of Hubble Space Telescope (HST) Guest Observer program 6672, we obtained a UV spectrum (1180 – 1680 Å in the rest frame) of the nucleus of NGC 7714 using the Goddard High Resolution Spectrograph (GHRS). Our analysis of the UV spectrum and a comparison with available X-ray, optical, and radio data was reported in Paper I. We also included in that paper an F606W image obtained with the Wide-Field Planetary Camera 2 (WFPC2) on the HST, taken from the HST archive.

In this paper, we extend our analysis into the IR. This wavelength range is particularly sensitive

to older, evolved stars, and to stars of all ages with heavy dust obscuration. We have obtained near-IR JHK_n images, and a K-band spectrum, which we present and analyze here. We also present a new near-UV image of NGC 7714 taken with HST. By combining the UV data from HST with optical and near-IR spectroscopy from the ground, we have accumulated high-quality spectra, spanning the range 1200 Å to 2.3 μm , for very nearly the same spatial regions of the galaxy. With photometric points from the X-ray to the radio, our spatial coverage spans several decades in frequency.

The new observations are presented in Sect. 2. In Sect. 3, the data are analysed with a focus on the morphological and structural information they contain for the central regions of NGC 7714. The coexistence of regions with very different properties, in particular in terms of extinction, already becomes evident in that section. The integrated spectrophotometric properties of the nucleus are analyzed in Sect. 4. We successively consider individual wavelength ranges, the full broad band energy distribution, and finally the full spectrum, and show that a variety of models remains consistent with even this amount of combined data. The predictions common to all successful models are highlighted and analyzed in terms of the nuclear morphology of the galaxy. Implications of our study for NGC 7714 itself and for studies of other starbursts are discussed in Sect. 5. The conclusions are given in Sect. 6.

2. Observations and data reduction

2.1. Spectroscopy at 2 μm

NGC 7714 was observed on the nights of 1996 July 26 and 28 UT, using the CGS4 spectrometer on the United Kingdom Infrared Telescope. CGS4 was equipped with a 256×256 InSb array. We used the 150 mm focal length camera with the 150 line/mm grating in first order. The slit was one pixel (1.22'') wide. In this configuration, four undersampled spectra were taken with the detector moved 0.5 pixels between each exposure. These were later merged to provide a properly-sampled spectrum with two pixels per resolution element, and pixel size of 6.5245×10^{-4} μm in the dispersion direction. Each individual exposure lasted 60 seconds. For each object exposure, an exposure of the nearby sky was also taken, to subtract the strong OH night sky lines. Our final co-added spectrum represents approximately 200 minutes on-source integration over the two half-nights of observing.

Our slit was placed at position angle 110° E of N, the same as one of the observations in González-Delgado et al. (1995). Our slit width was essentially the same as theirs. With the one assumption that the K-band peak and the optical peak are spatially coincident, we are observing almost exactly the same region of the galaxy.

IRAF and routines we wrote for IRAF were used for basic data reduction (flat-fielding, sky subtraction, combining undersampled spectra, wavelength and flux calibration, and removing the substantial tilt of the spectral lines caused by a failure in the slit mechanism). Careful attention was

paid to removing transient “hot” pixels, which were present in the data. We also carefully corrected for small DC offsets in the wavelength scale apparent over long timespans, probably caused by mechanical flexing. After a thorough examination, we believe we have properly accounted for all the instrumental effects.

OH night sky lines were used for wavelength calibration, using the wavelengths tabulated by Origlia & Oliva (1992). Because of the inevitable smearing induced by the fractional-pixel shifts needed to remove the flexing, we determined the actual spectral resolution of the data by measuring the OH line profiles in a co-added, pure-sky image produced from the sky images obtained between the object exposures, and processed in the same fashion. The resolving power, found from the full-width at half maximum of the OH lines, was ~ 1200 (250 km s^{-1}) at $2.2 \mu\text{m}$.

Spectra of A-type stars were used to remove atmospheric features and correct for instrumental response, since we could correct the only strong stellar feature expected, the $\text{Br}\gamma$ line, by fitting the line with a Gaussian and removing it from the stellar spectrum. The weather was not photometric on July 26, 1996, due to cirrus. To correct for this, the spectra were scaled to a common mean before co-adding them. We obtained absolute calibration from the 1996 July 28 data, when the weather was better. Observations of three flux standards showed the flux calibration to be accurate to $\sim 10\%$ in extractions 5 pixels wide in the spatial direction.

The final product was a 2-dimensional flux spectrum with useful dimensions of 500 (wavelength) by 49 (spatial) pixels, linearized in wavelength, and a corresponding error spectrum. Individual rows were then written out as ASCII files for further analysis using a stand-alone spectroscopic data reduction program described in Goldader et al. (1995).

2.2. JHK n imaging

We obtained near-IR JHK n images of NGC 7714 using the CASPIR camera on the Australian National University 2.3m telescope at Siding Springs Observatory on the nights of October 30 and 31, 1994. The K n filter is centered at $2.165 \mu\text{m}$ with full-width at half-maximum (FWHM) $0.33 \mu\text{m}$. The camera was based on a NICMOS3 256×256 pixel detector, with pixel size $0.5''$. The seeing, measured from pointlike objects in the final galaxy images, was $\sim 1.6''$ FWHM. The central $1'$ of our H-band image is shown in Fig. 1; the J and K n images are virtually identical in appearance.

The images were taken in photometric conditions, and two sets of observations were taken for each of two standard stars. When measured through apertures large enough to get almost all the flux from the stars ($12''$ diameter), the stellar photometry agrees to 0.02 magnitudes. Aperture corrections are significant for the smallest apertures we considered. Our photometry (with the flux standard and galaxy observed through identical apertures) is given in Table 1, and typically agrees at the 5 – 10% level with values from the literature. Our J & H magnitudes are effectively on the CIT system, but because of color terms between the K and K n filters, our K n magnitudes should be corrected upwards by ~ 0.1 magnitudes to be on the CIT system.

2.3. HST UV imaging

Our HST images of NGC 7714 were taken with the WFPC2 through the F380W filter. We used four exposures, 2×500 s and 2×400 s. Our final image (Fig. 2) is the combination of the four exposures as calibrated by the pipeline. The filter was chosen as a compromise, since we were intending to image the sites of the most massive stars, which are brightest in the UV, yet the sensitivity of WFPC2 drops at the shorter wavelengths. NGC 7714 was placed on the PC chip. The full WFPC2 field of view was large enough to include the nearby companion NGC 7715 as well. In Fig. 2 we reproduce the PC and WF frames at a cut to highlight the bridge between both galaxies.

3. Data analysis: the structure of NGC 7714

3.1. The ultraviolet appearance

In Fig. 3 we show the central $2.5'' \times 2.5''$ region of NGC 7714 in the F380W filter, and, for comparison, in the F606W filter from Paper I. A spiral structure is seen, starting to the North of the nucleus and extending first to the East, then to the South-East (where it reaches region A of González-Delgado et al. (1995), about $2''$ off the plotted area). At least 20 luminous star clusters are visible, with the brightest cluster in the very center. Anticipating the discussion further below, we note that the nuclear region is less reddened than its surroundings. Consequently, the brightness contrast between the nuclear and off-nuclear clusters becomes less pronounced after obscuration effects are taken into account. Surprisingly, the UV morphology of NGC 7714 from our new HST images is virtually identical to the morphology of the galaxy through the red F606W filter (see Paper I). There are dust lanes in and near the nucleus (Fig. 3), including one which goes across the apparent geometric center of the nuclear star-forming complex. The dark lanes are enhanced by making an “unsharp-masked” image, subtracting an image median-filtered through a box 30 pixels wide. We note that the brightest object in the nucleus, the cluster near position (0,0) in Fig. 3, does not seem to be at the geometric center of the star-forming complex, but appears to be located $\sim 0.3''$ NE of it. We have made a “color” image by dividing the F606W by the F380W image. The clusters are mostly very blue, and the dark lanes are redder, further indicating that they may truly be dust lanes.

The F380W magnitude of the nucleus of NGC 7714 rises quickly with aperture size up to aperture radii of about $2''$, at which point the brightness increases much more slowly (Table 2). As noted in Paper I, this sets the spatial scale of the starburst region at a few hundred pc.

3.2. The near-infrared appearance

In the infrared, NGC 7714 is dominated by a very small region centered on the nucleus. Nearly half the flux in a $9''$ aperture comes from the inner $1.74''$ diameter region. On larger scales, a bar is seen in the IR images, at the same PA of $\sim 143^\circ$ E of N as in optical images (González-Delgado et al. 1995). The giant H II region A is visible as a faint extension SE of the nucleus; region B is just barely distinguishable from the spiral arm in which it is found, whereas it is obvious in the HST images; and region C is readily visible SW of the nucleus. A higher-resolution (yet less deep) K-band image was kindly provided to us by D. Sanders. Taken in $1.1''$ seeing (FWHM) with $0.37''$ pixels, this image shows that the nucleus is resolved and has a deconvolved size of about $1.3''$ FWHM (with the FWHM of the point-spread function removed in quadrature from the FWHM of the nucleus in the image). No spatial structure is apparent in the near-IR continuum of the nucleus itself, though we attempted to deconvolve the image, and the nucleus may be slightly more extended in the N – S direction. A similar result was found recently by Kotilainen et al. (2000).

Red near-IR colors are often used as an indication of the presence of intermediate age populations (Persson et al. 1983, Silva & Bothun 1998). Near-IR colors derived from the data in Table 1 show a marginally significant radial gradient in $(J - Kn)$, the nuclear values being redder than those of the surroundings. A more significant gradient is found in $(H - Kn)$, while $(J - H)$ tends to be slightly bluer in the nucleus. Reddening is highly variable within the nucleus even in the near-IR (Kotilainen et al. 2000). After dereddening with $A_K \simeq 0.1$ (a typical value in the successful models described further on) and converting Kn to K , we find $(J - K)_o \simeq 0.75$. This value is consistent with a wide range of ages (e.g. Fig. 2 of Lançon 1999). The fact that the spatial color gradient is stronger in $(H - K)$ than in $(J - H)$ may be taken as a case in favour of an intermediate age nuclear component, as cool AGB stars preferentially contaminate the K band. However, anticipating the further discussion again, we note that colors consistent with the data can be obtained with a variety of combinations of stellar ages and extinction patterns. The observed gradient by itself cannot be simply transformed into a quantitative contribution of any particular subcategory of cool stars.

3.3. The infrared spectral image of the galaxy

A “central” spectrum of NGC 7714 was summed in a region 1×5 pixels ($1.22'' \times 6.10''$) in size, and is given in Fig. 4. The continuum resembles that of a late-type (K/M) star, complete with the strong CO absorption bands characteristic of such stars. Atop this are seen $\text{Br}\gamma$ ($\lambda 2.166 \mu\text{m}$), He I ($\lambda 2.058 \mu\text{m}$), and several H_2 emission lines. The line and continuum fluxes are strongest in the few pixels centered on the nucleus. However, continuum flux is also detected well away from the nucleus, along the “ring” SE of the nucleus, and also towards the NW. The $\text{Br}\gamma$ and He I lines are visible as the slit crosses the giant H II region B, NW of the nucleus. We also extracted the two strongest rows as the “nuclear” spectrum, which we will use later in conjunction with the optical and UV spectra (Fig. 5).

The fluxes and equivalent widths of the three brightest lines as functions of position along the slit are shown in Fig. 6. As can be seen, the equivalent widths of the ionized gas lines peak well off the nucleus, in H II region B. Interestingly, region B seems to have no significant IR continuum emission of its own — it is almost entirely an emission-line object. This is consistent with its prominent appearance in the HST F606W image (which includes the [O III], H α , and [N II] lines), yet inconspicuous IR appearance. The lower equivalent widths in the central region are evidence that the stellar flux is more concentrated towards the nucleus than the nebular flux. Emission line strengths are given in Table 3.

In Fig. 6 we also show the profile of our spectral image along the spatial direction. The profile was obtained by summing 55 pixels in the dispersion direction, between the 2.12 μm H $_2$ line and Br γ line, for each spatial row of the spectrum. The FWHM of the nucleus is about 3 pixels (3.6"). Spectral images of the flux standards showed typical spatial FWHM of 2 – 2.5 pixels (2.4" – 3") some of which was due to seeing, and some due to inaccuracies in centering the stellar image along the rows. This implies that the seeing-deconvolved FWHM of the galaxy is of order 2.2 – 1.7 pixels (2.6" – 2.0"). This is larger than the deconvolved size as seen in the IR images, probably from a combination of two effects. First, the long (60 seconds) galaxy exposures are subject to poorer seeing and greater image drifts than the 0.3 – 1 second stellar spectrum images. Second, the H II region A of González-Delgado et al. (1995) is present in our slit just SE of the nucleus, and this could also cause a wing on the spatial profile of the nucleus.

Numerous stellar absorption features are observed, the strongest being the ubiquitous CO band heads beginning at 2.3 μm . The strength of the CO index in the “central” spectrum corresponds to a photometric CO index of CO_{ph} = 0.13 magnitudes (Frogel et al. 1978), and a spectroscopic CO index of CO_{sp} = 0.17 magnitudes (Doyon et al. 1994). These values are typical of K0-K2 supergiants or late-K to early-M giant stars. In the “nuclear” spectrum, the CO index is CO_{ph} = 0.19 (CO_{sp} = 0.26), stronger than in the larger aperture, and implying the presence of cooler and/or more luminous stars. This is evidence for a gradient in the stellar population in the inner few hundred pc of the nucleus.

3.3.1. Near-IR rotation curves

The observed velocities along the slit as determined from the Br γ , He I, and H $_2$ $v = 1 - 0$ S(1) lines are shown in Fig. 7. The H α rotation curve from González-Delgado et al. (1995) is shown as a solid line. The agreement between the IR lines and the H α curve is excellent SE of the nucleus. To the NW of the nucleus, the Br γ line is systematically below the optical rotation curve. The discrepancy with Br γ might be due to the line profile being affected by a strong telluric line centered about 1 pixel redward of Br γ , as the Br γ line is redshifted into the night sky line. The gaseous velocity dispersions were too small to be derived at the spectral resolution of our data.

3.3.2. H_2 gas in and around the nucleus

An old question about the strong H_2 lines visible in the spectra of starburst galaxies is whether the gas is excited by shocks, or by the absorption of UV photons from the starburst (Goldader et al. 1997). The populations of the different energy levels of the H_2 molecules, reflected by the relative strengths of the different emission lines, can tell if the gas was excited by a non-thermal mechanism, such as shocks, or by the absorption of energetic photons. For comparison with our data, we refer to models S2 (for shock-excited gas, appropriate at high H_2 densities) and 14 (for lines arising from UV fluorescence in low-density gas) from Black & van Dishoeck (1987).

In Table 3, we give the measured strengths and upper limits (3σ , measured over a window 4 pixels wide in the dispersion direction) of the H_2 lines in the “nuclear” and “central” spectra. To examine the gas farther from the nucleus, where different physical conditions might prevail, we extracted the spectrum of the brightest three pixels along the slit, and subtracted this from our “central” spectrum. This gave us the sum of two pixels with significant signal in them, but not including the peak of the nuclear starburst. Though most of the lines in the different spectra were not detected, the ratios of the lines which were in fact seen (Table 4) are clearly different than for shock-excited, dense gas. The data are consistent with a mix of both shock-excited and UV-excited H_2 . This indicates that the total H_2 emission is dominated by the UV-excited gas, because that emits a smaller fraction of its total energy in the K-band lines than shock-excited gas.

3.4. Summary of the central morphology

At UV, optical and near-IR wavelengths, NGC 7714 has a rather compact core. The $\sim 2''$ “nucleus” that we focus on in this series of papers, emits about half of the light measured within a $\sim 10''$ radius. Another factor ≤ 2 is gained when including the whole galaxy.

While the near-IR continuum image is smooth in the nucleus, the UV and optical images show complex structure. It is instructive to compare them with the radio maps of Condon et al. (1982) and the $2.16 \mu\text{m}$ $\text{Br}\gamma$ emission map recently obtained by Kotilainen et al. (2000). Both show a double peaked morphology within our “nucleus”, with two maxima separated by about $1''$ along a NE-SW line. The best correspondance between all maps is obtained if region 2 of Kotilainen et al. (2000) is associated with the extended UV source at $\sim 2.2''$ to the East of the geometrical center, at the very edge of our images in Fig. 3. The brightest $2''$ in the near-IR continuum or in the UV then cover most of regions 1 and N of Kotilainen et al. (2000). With this assumption, the $\text{Br}\gamma$ and H_2 fluxes of these authors and ours are in excellent agreement. The brightest spot in the $\text{Br}\gamma$ map does not coincide with the bluest, brightest UV cluster. It is associated with less conspicuous UV sources, to the SW of the brightest one.

The evolution of the UV to near-IR flux ratio with aperture size was reconstructed from the magnitudes in Tables 2 and 1. It is shown in Fig. 8. $(F_{380W} - K_n) \simeq 3.06$ in the central $12''$.

Remembering the 0.1 magnitude difference between K and Kn , this agrees well with previous measurements. $(U - K) \simeq 2.9$ is obtained from the data summarized by Smith & Wallin (1992). The UV/near-IR flux ratio decreases steadily from $5''$ diameter apertures to larger ones, confirming the suspected trend of increasing stellar age or extinction with radius. Relatively red colors are obtained from our data for the “nucleus”. Although this 0.15 magnitude effect may be partly due to aperture mismatch, we estimate that it is significant. However, in view of the preceding discussion, it should not be interpreted as a simple gradient, but as the result of a patchy distribution of the luminous hot stars and the dust.

4. Understanding the composite nuclear spectrum of NGC 7714

Our efforts to fit the nuclear spectrum of NGC 7714 are based on a series of models from Pégase (Fioc & Rocca-Volmerange 1997) and the Starburst99 project (Leitherer et al. 1999). Starburst99 is an update of the work of Leitherer & Heckman (1995). The reader is referred to the three quoted papers for details. Both Pégase and Starburst99 utilize an evolutionary synthesis technique, with the former emphasizing the physics of cool stars (in particular the inclusion of the thermally pulsing AGB; Lançon et al. 1999), and the latter that of hot stars. In both approaches, models of the emission from starburst stellar populations are calculated as functions of age, the initial mass function slopes, lower and upper mass cutoffs, and stellar evolutionary tracks of selected metallicities. Continuum emission from ionized gas is always taken into account, with the assumption that no Lyman continuum photons escape from the galaxy. As all stellar populations considered will have total stellar masses larger than $10^6 M_{\odot}$, the effects of stochastic fluctuations in the numbers of luminous stars can be neglected (Lançon & Mouhcine 2000, Cerviño et al. 2000). Unless otherwise stated, a Salpeter IMF extending from 1 to $80 M_{\odot}$ is used as it was done in Paper I.

We attempt to arrive at the simplest possible models explaining the spectrum of the very center of NGC 7714. As we will discuss, model solutions are not unique. In order to further restrict the range of satisfactory models, the UV to near-IR SED is combined with information from longer and shorter wavelengths. We aim at identifying the common features of the collection of simple models that are consistent with the data.

4.1. The composite nuclear spectrum

We have used our data to construct the multiwavelength SED of the inner $\sim 330 - 380$ pc ($1.74'' - 2''$) of NGC 7714. For the UV, we have used the GHRS spectrum of Paper I, which was obtained through the $1.74'' \times 1.74''$ Large Science Aperture. For the optical spectroscopy, we averaged two spectra extracted by González-Delgado et al. (1995), one in aperture $1.2'' \times 2.1''$, and the other in $1.2'' \times 3.5''$. This gives us an effective aperture a bit larger than the GHRS aperture. We scaled up the optical spectrum fluxes by a factor of 1.6 to account for point-source losses

through the narrow slit (see the note in Paper I). We performed photometry on our HST images through apertures $1.74''$ in diameter. We used the “nuclear” K-band spectrum in an aperture $1.2'' \times 2.4''$. From our IR images, we obtained photometry at JHK n through circular apertures $1.74''$ in diameter, to approximate the GHRS aperture.

Though we have tried to obtain data through similarly-sized apertures, it is important to note that slight differences in aperture position, size, and photometric calibration must cause some normalization differences between the spectra. We estimate those differences are at about the 10 – 15% level at most.

4.2. Model boundary conditions

Several basic constraints must be considered while fitting the multiwavelength nuclear spectrum of NGC 7714. These constraints result from our previous studies (Paper I), from the literature and from the above data analysis.

1. The nuclear chemical composition is close to solar. Our models are made under this assumption (but see Sect. 4.7 for a discussion).
2. The observed UV spectrum in the GHRS aperture is best described as an instantaneous burst population of age ~ 4.5 Myr with reddening of $E(B - V) \approx 0.11$. Of this reddening, about 0.08 magnitude is from the Milky Way, and 0.03 magnitude is intrinsic to NGC 7714.
3. The reddening to the nuclear ionized gas, determined from the Balmer decrement, is $E(B - V) = 0.21$. About 0.13 magnitude is intrinsic to NGC 7714.
4. A strong 4000 Å break is present in the optical spectrum, implying that a significant part of the optical spectrum is due to a population older than $\sim 10^8$ years.
5. A luminous near-IR continuum is present, and the conspicuous CO bands at $2.3\mu\text{m}$ show that this continuum is due to luminous cool stars.
6. The IRAS far-IR luminosity is $L_{\text{IR}} = 3 \times 10^{10} L_{\odot}$. L_{IR} approximates the total bolometric luminosity and exceeds the UV luminosity in the IUE aperture by about an order of magnitude (Heckman et al. 1998). The UV luminosity in the GHRS aperture is another factor of ~ 2 smaller (Paper I). One may a priori expect the nuclear stars to be responsible for 10% – 50% of the IRAS flux. Noting that no direct spatial information is available at the longest IR wavelengths, this is consistent with the recent $12\mu\text{m}$ maps obtained with the Infrared Space Observatory (O’Halloran et al. 2000).
7. The ROSAT soft X-ray luminosity of NGC 7714 is $4.4 \times 10^{40} \text{ erg s}^{-1}$. Stevens & Strickland (1998) interpret this X-ray flux as due to thermal emission from supernova powered, hot

bubbles and/or a galactic wind. The non-thermal 20 cm flux reported by Weedman et al. (1981) is most likely related to the same phenomenon.

Although our goal is to fit a co-spatial region in the nucleus of NGC 7714, we recall the properties of the spectrum measured in the IUE aperture. That spectrum suggests a population of OB stars, possibly mixed with some older stars. Typical values for the galaxy’s $E(B - V)$ are around 0.3.

4.3. Dust obscuration and emission

The far-IR emission of NGC 7714 shows that dust cannot be neglected in the study of the energy distribution of the galaxy. The presence of dust will affect the shapes of modeled spectral energy distributions, in a way that depends both on the nature of the grains and on their spatial distribution relative to the sources of light. Puxley & Brand (1994) used optical and near-IR recombination lines to examine the dust obscuration towards ionized gas in NGC 7714. They found that the line ratios were adequately fitted by a simple foreground screen of dust with $A_V = 0.86 \pm 0.13$ magnitudes ($E(B - V) = 0.28 \pm 0.04$). Since the simplest possible extinction geometry fitted their observations quite well, they felt no need to favor the more complex alternatives they had explored.

In our attempts to fit the SED of NGC 7714, we have systematically accounted for the 0.08 magnitudes of foreground Galactic extinction using a standard extinction curve (Howarth 1983). For extinction intrinsic to NGC 7714, we generally use the starburst obscuration curve of Calzetti et al. (2000), in the framework of the foreground screen geometry consistent with the derivation of that curve. This seems reasonable in the light of the results of Puxley & Brand (1994), and avoids introducing more free parameters associated with more complicated extinction geometries.

We do however also invoke different choices of the geometry and the extinction law. Spatial variations of the extinction are to be expected in NGC 7714: dust lanes cross the images, extinction in the GHRS and IUE apertures differ. The obscuration curve of Calzetti et al. (2000) was derived empirically from a sample of integrated spectra of starburst galaxies, in order to provide a tool to be used in a screen geometry formalism for average starbursts. It implicitly accounts for both wavelength dependent dust properties and typical dust distributions. The distribution appropriate for the central few arcseconds of NGC 7714 may differ from this average picture.

Our predictions for the far-IR emission are based on a simple energy budget. We compute the difference between the model SEDs before and after extinction has been applied, integrate the difference over wavelengths and assume that this energy is reradiated by the dust in the far-IR. We note that this method assumes symmetry in the galaxy structure. For instance, it underestimates the far-IR flux if UV-optical light escapes towards the observer more easily than in any other direction from the source, and it overestimates the far-IR flux if the line of sight happens to cross a particularly dense foreground cloud. The wavelength dependence of extinction ensures that the

hottest of the reddened stars contribute most strongly to the predicted emission. The emission temperature of the dust is known to depend on the grain size distribution and on the proximity of the grains to the hot stars (Helou 1986, Mazzarella et al. 1991). This also determines which fraction of the dust radiation was actually measured by IRAS. However, the absence of spatial resolution in the far-IR already results in such a large uncertainty on the nuclear emission that it is not justified to attempt to model the far-IR energy distribution more precisely.

4.4. The nucleus approached from three wavelength ranges

4.4.1. Results from the GHRs UV spectrum

Paper I showed that a 5 Myr old instantaneous burst (ISB) with an intrinsic $E(B - V)$ of 0.08 provides the best representation of the stellar lines seen in the GHRs UV spectrum. The corresponding reddened model spectrum, scaled to match the GHRs spectrum, accounts for about $30 \pm 3\%$ of the continuum flux at 5500 \AA and only about 3% of the K-band continuum. This population produces about 1% of the galaxy’s far-IR luminosity if the dust optical depths around it does not exceed the optical depth on our line of sight. In the more likely case of an irregular dust distribution, the burst would provide 2 – 4% of the far-IR light (4% corresponds to the bolometric luminosity of this burst population).

The percentage contribution of the 5 Myr burst at near-IR wavelengths can be increased with dust distributions more complex than a screen. But no reasonable adjustment of the UV to near-IR SED can be obtained with this single burst age. Such adjustments would require more than 99% of the young stars to be heavily obscured, leading to unrealistic amounts of far-IR emission (besides being incompatible with the spectroscopic information in the optical and near-IR). Thus, the young burst seen in the UV does not by itself explain the energy distribution of NGC 7714’s nucleus.

The UV spectrum is marginally consistent with models for ISBs slightly older than 5 Myr or with continuous, constant star formation (CSF). Again, none of these, combined with a simple foreground screen extinction, can fit the observed colors. Adjustments of the broad band energy distribution with CSF models and modified dust properties can be obtained, but since they do not follow directly from the UV analysis their discussion is postponed to Sect. 4.5.

The conclusion from the UV analysis, placed in the context of the UV-through-IR SED of NGC 7714, is that the recent star formation event, though dominant at short wavelengths, is not the only relevant star-formation episode to be considered, even when focusing on the central 330 pc of the galaxy. What is most likely required is one population of age ~ 5 Myr, and at least one older population rich in cool stars and weak in ionizing flux.

4.4.2. *Results from the Balmer line profiles and the Balmer jump*

The optical spectra of starbursts are dominated by nebular emission lines, but they can also display the H and He I absorption lines formed in the photospheres of O, B, and A stars. The reason why these features can indeed be detected in absorption in starbursts such as NGC 7714 is that the equivalent width of this absorption is constant throughout the Balmer series, while the emission line strengths decrease rapidly with decreasing wavelength. The strengths of the Balmer and He I absorption lines show a strong dependence on effective temperature and gravity, and therefore provide constraints on starburst and post-starburst ages (González Delgado & Leitherer 1999, González Delgado et al. 1999). In the spectrum of a coeval population, the absorption equivalent widths of these lines increase with time until they reach a maximum at ages of 300 – 500 Myr, and decrease afterwards. Spectra for older and younger populations can also be distinguished through the shape of the “continuum” in the Balmer jump region, between 3720 and 3920 Å: the rather abrupt jump seen shortward of 3800 Å at young ages turns into a flatter but broader slope later on (e.g. Fig. 2 of González Delgado et al. 1997).

For an instantaneous young burst (a few Myr old), the predicted Balmer lines are much weaker than those observed in the nucleus of NGC 7714. This confirms the need for a composite nuclear stellar population.

A variety of star formation histories are consistent with the absorption line profiles of the normalized optical spectrum of the nucleus of NGC 7714. Among them, a CSF model with a duration of a few 100 Myr, or combinations of a 4 – 5 Myr old burst with populations a few 100 Myr old. However, some of these fail to simultaneously reproduce the shape of the “continuum” in the Balmer jump region. There is no abrupt Balmer jump in the NGC 7714 spectrum. In the satisfactory models, the relative fraction of young (< 100 Myr old), hot stars must be smaller than in constant star formation models, unless star formation lasts for more than ~ 800 Myr.

4.4.3. *Results from the near-IR spectrum*

As mentioned in Section 3.3, the near-IR spectrum shows numerous stellar absorption features. The CO bands are relatively strong, implying the presence of red supergiant stars, but not strong enough to exclude a significant contribution from less luminous late-type giants. These can be predominantly upper AGB stars if the typical ages lie between 10^8 and 10^9 yr, or RGB stars for older ages.

After a few 100 Myr of evolution, about 50 % of the K band light of an instantaneous burst population originates from upper AGB stars. The light thus carries the spectral signatures of long-period variables that may be oxygen-rich (e.g. Miras) or carbon-rich (Lançon et al. 1999). An inspection of the stellar spectra of Lançon & Wood (2000) shows that the metal lines identified in the nucleus of NGC 7714 are present with various strengths in oxygen-rich late-type stars of

all luminosity classes, including Miras. In contrast, they are not seen in C stars, where blends of many other features mainly due to C₂ and CN make the K band pseudo-continuum much more irregular (at the resolution of our data). None of the typical C star features is obvious in the NGC 7714 spectrum (Fig. 9, top). Thus, although C stars can be more numerous than Miras in particular circumstances (e.g., at low metallicity and a metallicity-dependent range of ages; Iben & Renzini 1983; Groenewegen & de Jong 1993; Mouhcine & Lançon, in preparation), we do not need to take this possibility into account here. Many variable O-rich AGB stars show strong H₂O absorption bands around 1.9 μm, whose wings extend up to 2.1 μm. The resulting change in the apparent continuum slope is not seen in our NGC 7714 spectrum (Fig. 9, second from top). However, we note that at wavelengths below 2.1 μm the correction for telluric H₂O absorption is important, possibly affecting the flux levels with larger errors. In addition, because of uncertainties in the evolutionary tracks and the effective temperature scales of the upper AGB, the quantitative predictions of the synthesis models regarding the strength of the water bands are still uncertain.

In summary, the K band spectrum is consistent with a variety of combinations of red supergiants, AGB stars and RGB stars. It is unlikely that a single red supergiant dominated population (e.g., an ISB with an age of a few 10⁷ yr) or a single AGB dominated population (e.g., an ISB with an age of several 10⁸ yr) can quasi-exclusively be responsible for the near-IR light. A similarly open-ended conclusion was drawn from a near-IR spectrum at shorter wavelengths by González-Delgado et al. (1995), on the basis of the calcium triplet absorption lines.

4.5. Simple star formation histories that adjust the broad band SED

Pluralitas non est ponenda sine necessitate (Occam’s Razor) — yet a single coeval young population has been excluded as a representation of the nucleus of NGC 7714 in the previous sections. The next, more complex model has constant star formation over some period of time.

Gordon et al. (1997) studied the starburst in NGC 7714 (through larger apertures than ours) using a Monte-Carlo radiative transfer model with different dust distributions relative to the stars. They found that, among others, a long lasting CSF model with a duration of about 1 Gyr could represent the data, assuming SMC dust properties and an inhomogeneous shell geometry (dust shell with higher density clumps). Our aim is not to explore all possible dust geometries. However, the degeneracy between intrinsic SED properties and obscuration properties mentioned by Gordon et al. (1997) cannot be ignored. It is indeed possible to fit the broad band energy distribution even of the central 2'' with constantly star-forming models when the dust distribution is allowed to differ from a simple screen. The HST images and color maps clearly allow for some complexity. For instance, the SED is reproduced very well after 1 Gyr of constant star formation, if nearly half the stars are hardly reddened at all and the other half are located behind dust screens with optical depths of the order of 1.5 (Figure 10). This configuration predicts that $4 \times 10^9 L_{\odot}$ of stellar light is absorbed by dust, with a predominant contribution from the hotter of the coexisting stars; the nuclear 5'' then provide about 10 % of the total far-IR luminosity of the galaxy, a fraction consistent

with the galaxy morphology as summarized in Sect. 4.2.

How much can the age of the CSF model be varied, if only dust is allowed to modify the SED in order to match the broad band photometry? For CSF durations larger than 5 Gyr, the intrinsic ($UV - V$) color of the stellar population becomes redder than observed in NGC 7714. Older models cannot be considered (scattering may reduce the reddening effect of dust, but “blueing” in the optical is not expected; Witt et al. 1992). Already at 5 Gyr, the contribution of the reddened component is so low that only 2% of the far-IR light of the galaxy are accounted for in the nucleus. Going towards lower ages, CSF models as young as a few 10^7 yr reproduce the observed colors, with adequate combinations of dust optical depths. However, the large number of hot obscured stars then tends to produce too much far-IR flux. Both the old and young extreme CSF histories considered also produce inadequate spectral signatures in the Balmer region. If star formation is assumed to have been constant in the nuclear area but dust reddening is allowed to vary with the line of sight, ages between about 800 Myr and about 3 Gyr match the colors and the optical absorption features, and are also consistent with the near-IR spectrum.

The stellar features observed in the GHRS UV spectrum, however, are so strong that consistency with a long episode of constant star formation is only marginal. A larger relative UV contribution of stellar populations with an age of the order of 5 Myr is favored. Model options based on this constraint from Paper I are explored in the following section.

4.6. Adjusting both the colors and the spectra

As soon as we stop limiting ourselves to single ISB or CSF models but consider composite populations, the number of model parameters increases dramatically. Throughout the following, we maintain the constraint that the UV continuum of the GHRS aperture predominantly arises from a 4.5 – 5 Myr old instantaneous burst with very low intrinsic reddening. A “component” of the composite population is defined as group of stars that can be represented with a common, simple star formation history: an ISB, a CSF, or an exponentially decreasing star formation rate. For simplicity, a same amount of obscuration is assumed to affect all stars of a same component.

In practice, we proceed the following way. Various families of models are considered successively, defined by the number of stellar populations considered in addition to the GHRS burst (limited to 2 or 3), the type of star formation history in each (e.g. ISB, CSF, exponential), and the adopted extinction prescription. For each family, we step through component ages. An automatic optimization procedure (based on a quality-weighted χ^2) then determines the most adequate extinction values and relative contributions for the components. By visual inspection, we reject solutions that are obviously inconsistent with the data; the others are included in the discussion. The choice of a soft rejection criterion is dictated by the uncertainties in the observations, and in particular in the relative calibration of the individual spectral segments.

In order to identify global properties of the missing stellar components, we first consider models

with either *one* additional burst or *one* additional constantly star-forming component. For a given age of the second component, both its relative contribution to the light and the amount of reddening it is affected by are obtained by optimizing the fit to the UV through near-IR spectrum. The best fits obtained with the assumption of constant star formation qualify as good, while the additional burst assumption merely provides a marginally acceptable fit, in particular around 4000 \AA and for the CO bands. Both types of models provide satisfactory amounts of far-IR emission. The two classes of results are shown schematically in Fig. 11: either a massive starburst occurred about 300 Myr ago, or star formation occurred continuously over about 800 Myr at a rate of about $0.6 M_{\odot} \text{ yr}^{-1}$.

Despite their differences, the two classes of selected “two-component” models have an important common feature: over timescales of a few to several 10^8 yr , $5 - 7 \times 10^8 M_{\odot}$ of stars were formed in the observed aperture (in the $1 - 80 M_{\odot}$ mass range). The presence of more stars in the age range of $10^7 - 10^8 \text{ yr}$ is, in the constant star formation scenario, compensated for with an older age, in order to adjust the spectrum around the Balmer jump. The 5×10^6 to $10^7 M_{\odot}$ of stars formed over the last 5 Myr in both cases are only a small part of a more important star formation episode.

What, then, was the history of star formation over the last several 10^8 yr ?

A simple two-burst model is most probably inadequate. In addition to providing a marginally acceptable fit to the spectrum, it requires fine tuning to explain the observed radio emission: the supernova rate predicted is too low because the 5 Myr old population is still too young and the 300 Myr old burst is too old. As seen in the HST images, compact very blue knots are found at several locations. No obvious feature of the galaxy explains why they should have formed simultaneously 5 Myr ago after a long period of quiescence, whereas they can quite naturally be seen as the youngest components of a more extended process of star or star cluster formation, for instance as a result of the gravitational interaction with NGC 7715.

On the other hand, a timescale of 800 Myr is long compared to estimates of the interaction timescale with NGC 7715 (Smith et al. 1997). Shortening the star formation timescale without producing too many ionizing photons and degrading the fit around the Balmer jump, requires the partial suppression of very recent star formation (Sect. 4.4.2). In this context, the most natural explanation for the observed properties of the nucleus of NGC 7714 is a globally decreasing star formation rate with an initiation a few 10^8 yrs ago. The data are consistent with a smooth, exponentially decreasing star-formation rate with an exponential timescale of $50 - 100 \text{ Myr}$, or with a series of burst events (as little as three may be sufficient) of decreasing total masses. In the latter case, a $15 - 50 \text{ Myr}$ old burst provides the required supernova rate, a significant contribution of red supergiants to the near-IR flux, and usually a dominant fraction of the far-IR luminosity; the intermediate age burst (a few 100 Myr old) adjusts the spectrum in the 4000 \AA region, contributes significantly to the near-IR light because of upper AGB stars, and participates at a lower but non-negligible level to the heating of dust. Examples are shown schematically in Fig. 12, and an illustrative fit is plotted in Fig. 13.

Finally, a contribution of a pre-existing, old population may be expected in the nucleus of

a spiral galaxy. The amount of this contribution depends strongly on the model adopted for the underlying spiral. And very little is known a priori on the relative enhancement in the mass of stars a starburst can produce. The spectrum itself provides constraints. Old populations have much redder colors in the optical range than observed in the nucleus of NGC 7714. They cannot be dominant; a strong contribution from an intermediate age population (less than 1 Gyr in age) remains necessary. A large number of tests were performed, in which the star-formation history of the underlying spiral was represented with a Schmidt law, as appropriate for Sa-type galaxies. It is indeed possible to obtain satisfactory adjustments of the nuclear data with a significant contribution of the underlying population (e.g. Fig. 14). The duration of the recent star-formation episode can then be relatively short (down to about 200 Myr), as the pre-existing stars help providing a good fit around 4000 Å. With star-formation durations larger than 200 Myr, however, the upper AGB stars help in reaching the observed near-IR flux level and less fine-tuning is required.

The most important effect of the underlying population is to reduce the mass of stars produced by the intermediate age events from typically $3 - 4 \times 10^8 M_{\odot}$ to about $1 - 2 \times 10^8 M_{\odot}$. The global star formation scheme however remains valid. Most of the far-IR flux is due to the hot stars of the recent events, though a (model dependent) contribution from the underlying population is present (current star formation is not nil in the underlying spiral models). The mass of stars in the underlying population can exceed the mass in recent stars. It reaches about $10^9 M_{\odot}$ only in a rather extreme category of models where a very old, nearly constantly star-forming spiral population would totally dominate the near-IR emission. This would help explaining the very regular near-IR continuum images of the nucleus, but is difficult to reconcile with the strength of the observed near-IR absorption features. We conclude that the mass of stars formed over the last few 10^8 yr is at least 10% of the total stellar mass present in the aperture, and we favor values around 25%.

4.7. Further consistency checks and plausible model variants

In the study described above, we have assumed that the stellar populations of NGC 7714 have solar metallicity. As the nebular lines suggest slightly subsolar abundances (Paper I), we have also systematically searched for models at half-solar metallicity. We note that these must be treated with some caution for supergiant-dominated post-starbursts: current stellar evolution tracks produce a smaller number ratio of red to blue supergiants at lower metallicities, while star counts favor the opposite trend (Langer & Maeder 1995; Origlia et al. 1999). A more robust prediction is that subsolar populations have bluer red giant and asymptotic giant branches. A global consequence of the use of subsolar tracks is the need for more reddening to adjust the observed SED. It becomes more difficult to explain the large near-IR flux unless some of the cool stellar populations are affected by as much as 1.5 magnitudes of visual extinction (screen model). However, albeit with differences in the precise values of the model parameters, we find that the range of successful models at half-solar metallicity essentially overlaps with those found with solar abundances. The predicted

far-IR emission is larger, but not enough to modify our conclusions. While the optical emission line ratios at $Z_{\odot}/2$ clearly favor an instantaneous 5 Myr old burst as the origin of the Lyman continuum photons (Paper I), both ISB and CSF models predict ratios consistent with the data at the solar metallicity used here.

A further check on the validity of our fits is how well we can reproduce the observed hydrogen recombination line equivalent widths. As an illustration, we will focus on the 3-burst model of Fig. 13 (we note that the presence of the underlying population does not modify the reasoning and results). The $H\beta$ equivalent width ($W(H\beta)$) is measured to be $\sim 26 \text{ \AA}$ in the optical spectrum we used, and $W(\text{Br}\gamma)$ is 21 \AA in our K-band spectrum. In our model, the UV-bright, 5 Myr population is responsible for about 25% of the continuum at $H\beta$, and 3% of the continuum at $\text{Br}\gamma$. The emission line fluxes of the 200 Myr population and the 10 Myr population are negligible. The contributions of the other stellar populations dilute the equivalent widths from the youngest population to 20 \AA at $H\beta$ and 5 \AA at $\text{Br}\gamma$. However, the emission line equivalent widths change strongly between 3 and 5 Myr, and if the age of the youngest component is taken as 3 Myr instead of 5 Myr, then the diluted equivalent widths become 55 \AA at $H\beta$ and 14 \AA at $\text{Br}\gamma$. Hence, we can trade off small age differences against fractional contributions of the youngest component at any particular wavelength. We can account for the observed $H\beta$ equivalent width this way, but the predicted $\text{Br}\gamma$ equivalent width is still too small by up to 50%.

Extinction can solve this apparent weakness of the model in various ways. It has often been stated that the gas emission associated with a starburst is reddened more than SED (Calzetti, 2000). If this is the case in the nucleus of NGC 7714, the agreement with the ratio of the $\text{Br}\gamma$ to $H\beta$ equivalent widths is improved, but the deficiency of $\text{Br}\gamma$ photons remains. More likely, there may be additional young stellar populations, obscured enough to not contribute significantly to the UV SED (a requirement imposed by the blue UV colors). The reddened line emission associated with these stars enhances the equivalent widths of the Brackett lines more than those of the Balmer series. This configuration explains both the missing $\text{Br}\gamma$ flux and the fact that the line ratios lead to a higher $E(B - V)$ than the UV continuum. It is fully consistent with the nuclear morphology discussed in Sect. 3.4. The hidden young populations must be able to increase the $\text{Br}\gamma$ equivalent width by the necessary factor without degrading the fit to the SED (in particular in the UV and around the Balmer jump). We find that they may contain up to 4 times the stellar mass of the burst actually seen in the UV, and would be typically be affected with $E(B - V) \simeq 0.35$. The modified models remain consistent with the far-IR constraints ($10^{10} L_{\odot}$ of far-IR light are predicted for the nucleus). We emphasize that the presence of the hidden stars does not drastically modify the scenarii we have already considered. The most recent star formation remains a small part of a longer star formation episode. In some of the previously discussed successful models, the GHRS burst was combined with continuous star formation components: the latter can also provide the obscured hot stars.

In Paper I, the bolometric luminosity of the starburst *seen* in the UV continuum of the GHRS aperture was estimated as $5 \times 10^9 L_{\odot}$, almost 10 times less than the IRAS luminosity. The range

of models suggested here agrees with this result. That young starburst population can at most be responsible for a few $10^9 L_{\odot}$ of dust emission in the far-IR, the exact value depending on the distribution of dust around those stars, in directions other than our unobscured line of sight. The hottest of the stars associated with the intermediate age populations, which formed stars over the last few 100 Myr and are more obscured, typically account for $3 - 6 \times 10^9 L_{\odot}$ of dust-processed far-IR light, i.e. less than 20% of the IRAS luminosity. A contribution of up to 50% might be achieved without too much stretching if, as suggested by the emission line analysis, additional obscured young populations are present. In any case, a significant fraction of the far-IR luminosity is expected to come from the stellar populations distributed outside the nucleus. As the IUE flux at 1500 Å is about twice the GHRS flux and the IUE continuum is globally affected by reddening, this is a reasonable conclusion. Only high spatial resolution in the mid/far-infrared would allow us to derive tighter constraints from the energy budget.

We showed in Paper I that the 5 Myr burst seen in the UV could account for the observed X-ray and non-thermal radio emission of the galaxy if it produced supernovae and supernova remnants which have unusual (but not implausible) properties. The 5 Myr burst is associated with a supernova rate of 0.007 yr^{-1} . If the supernovae power the X-ray luminosity of $6 \times 10^{40} \text{ erg s}^{-1}$ and the non-thermal radio luminosity of $4 \times 10^{38} \text{ erg s}^{-1}$ (Weedman et al. 1981), radiation losses must be small and the supernova remnants must be excessively luminous. An underlying obscured population of age tens of Myr greatly alleviates these constraints. For instance, the 3-component model in Fig. 13 has a 20 Myr old population producing supernovae at a rate of 0.07 yr^{-1} , i.e. an order of magnitude larger than the supernova population from the unobscured 5 Myr burst. This rate is very similar to the one derived for the *IR-bright* starburst archetype M 82: Ulvestad & Antonucci (1994) find a supernova rate of $\sim 0.1 \text{ yr}^{-1}$ in M 82. M 82 and NGC 7714 have the same bolometric luminosities of $3 \times 10^{10} L_{\odot}$. If they are powered by starbursts, and if the starburst properties are similar, the supernova rates should be similar as well. The proximity of M 82 permits detailed radio mapping and relatively accurate supernova and supernova remnant estimates. NGC 7714 is too distant for such studies. The *measured* supernova rate in M 82 and the *predicted* rate in NGC 7714 agree. Since the predicted rate follows from our multi-component fitting of the entire SED, we can have some confidence in the overall sanity of the models.

5. Discussion

A wide range of models has been shown to agree with the available information on the SED of the central $\sim 330 \text{ pc}$ of NGC 7714. Yet, the global scheme of all of them is similar, and in good agreement with the current understanding of starburst galaxies: star formation in a starburst partly occurs in compact brief bursts and may globally be spread over regions of several 100 pc in space and several 100 Myr in time, mimicking a relatively continuous and extended star-formation episode.

Smith & Wallin (1992) and Smith et al. (1997) used dynamical simulations to study the

NGC 7714/7715 system. They estimate that 100 Myr have elapsed since closest approach. As confirmed by J. Wallin (private communication), the scaling uncertainties in the dynamical models would not allow us to stretch the interaction timescale to much more than 200 Myr, which is among the very shortest of the star formation timescales of satisfactory spectrophotometric models. We interpret this as evidence that the latest interaction, which certainly played an important role in triggering the most recent star formation, probably followed other events that had already favored enhanced star forming activity earlier on. A second pass of NGC 7715 is one of the scenarii worth further investigation in the future.

Which data are most important in constraining the many evolutionary model parameters? A vast range of models was found capable of reproducing the *broad-band* energy distribution, in particular because of the strong degeneracy between intrinsic colors and reddening introduced when the dust distribution is allowed to be complex (as suggested by the images). The parameter space was further narrowed using (i) the stellar lines in the UV — because they were strong enough to imply a predominant 5 Myr old population at short wavelengths, (ii) the spectrum around the Balmer jump — because the absorption lines and the continuum are sensitive to age, and thus to the relative contributions of various components, in the age range relevant to NGC 7714. The K band spectra, then, were used for consistency checks: none of the specific spectral signatures of red supergiants, AGB stars or red giants happen to be strong enough in NGC 7714 to imply the predominance of one of these types, and many composite populations thus provide adequate features. Once the gap in the data between 0.95 and 1.95 μm will have been filled, the shape of the complete near-IR spectrum, that is determined to a large extent by molecular features, should rule out some of the models we must still take as acceptable here.

It is instructive to locate the global and central data for NGC 7714 on the diagram of Meurer et al. (1999), which shows a correlation between the ultraviolet spectral index β ($f_\lambda \propto \lambda^\beta$ in the IUE spectral range, as defined by Calzetti et al. 1994) and the ratio of far-IR to UV flux, for large aperture observations of a sample of starburst galaxies of various types. This is done in Fig. 15. When observed through large apertures, NGC 7714 follows the main trend (Meurer et al., 1999). Recall that about half the IUE flux comes from the central ~ 330 pc, and that 10 to 50% of the far-IR flux originates there. This places the central region off the relation, further than any of the global galaxy data of the sample of Meurer et al. (1999). For NGC 7714, the global properties clearly are the result of large scale averaging of very diverse local properties. Along individual lines of sights, random effects of the dust distribution are large; detailed UV to far-IR energy budgets are made uncertain by unknown losses and gains through scattering on gas and dust. We extrapolate this conclusion, and suggest that the smoothing effect of observations through large apertures plays an important role in producing the relation of Meurer et al. (1999).

Should one expect searches to find whole galaxies at locations in the diagram close to NGC 7714's central regions? Obtaining as negative a value of β would require a very prominent young population to lie essentially in front of any dust or in a dust hole; this is not impossible, but probably rare. Objects above the main trend at $\beta \simeq -1$ would be less surprising, as that is an expected location

when significant amounts of dust are mixed among the stellar populations: at each wavelength, one then sees down to optical depths of order one, which results in $\beta \simeq -1$, rather independently of the (large) far-IR emission. Meurer (2000) indeed finds that the ultraluminous infrared starburst galaxies lie in that area, with the objects studied to date having $-2 \leq \beta \leq -0.5$ and $\log(F_{\text{FIR}}/F_{\text{FUV}}) \geq 2$; we would not be surprised if the gap between the two current galaxy samples in the diagram were eventually filled.

6. Conclusion

A supposedly simple system as the proto-typical starburst nucleus in NGC 7714 turns out to be rather complex. High resolution imaging reveals highly irregular structure even within the central ~ 330 pc. In the study of the energy distribution of this region, star formation history, geometry and grain properties conspire against evolutionary synthesis models. The degeneracy is only partly broken even when data throughout the electromagnetic spectrum are combined. However, several significant results follow from the collection of models that satisfactorily reproduce the photometric and spectroscopic data:

- The nuclear ~ 330 pc of NGC 7714 have been forming stars off and on over the past several hundred Myr, at an average star formation rate of the order of $1 M_{\odot} \text{ yr}^{-1}$. About 5 Myr ago, an enhancement over this average rate by a factor of a few has occurred.
- The mass of gas transformed into stars over the last several 100 Myr amounts to $1 - 5 \times 10^8 M_{\odot}$ (in the $1 - 80 M_{\odot}$ mass range, with a Salpeter IMF). Of these, $4 - 20 \times 10^6 M_{\odot}$ were processed within the most recent star formation episode (the exact value depends sensitively on the dust distribution).
- The duration of the extended star formation episode determined spectrophotometrically is longer than the 110 Myr elapsed since closest contact with NGC 7715, according to the dynamical study of Smith & Wallin (1992). Only a small subsample of our satisfactory models is consistent with a timescale of 200 Myr, that would be within the uncertainties of the dynamical estimate. While the last interaction may have triggered the most recent star formation, it is unclear what first initiated starburst activity.
- The spectrophotometric data place (model dependent) limits on the contribution of the underlying population. Assuming the same IMF as for the burst and a standard spiral star formation law, we find an upper limit of about $10^9 M_{\odot}$ for this contribution. Thus, the recent star formation episodes have enhanced the stellar mass in the nucleus by at least 10 % (most models suggesting about 25 %).
- The UV luminosity is due to leakage of a small fraction ($\sim 10\%$) of the stellar photons, from a central cluster that happens to be unobscured, or from a central hole in the ISM.

- In the GHRS aperture, the stars younger than ~ 5 Myr (among which those actually seen in the UV), do not suffice to explain the far-IR emission. A large contribution from intermediate age stars ($\sim 10^7$ yrs old and not seen in the UV) or, alternatively, significant photon exchanges with regions outside the aperture (through scattering on gas or dust) are essential.

The HST images of the center of NGC 7714 show 10 – 20 individual bright spots, possibly clusters. None of these is dominant (in bolometric light) to be identifiable as the galaxy nucleus. The stellar populations that dominate at UV, optical and near-IR wavelengths have different ages and different amounts of extinction. This spectrophotometric result is in excellent agreement with multiwavelength high resolution imaging, which shows, for instance, that the UV continuum and the Br γ line emission maxima do not coincide in space. It is not surprising that values of $E(B - V)$ determined from Balmer lines or from the continuum at various wavelengths differ. The light contribution of the underlying population is strongest in the near-IR, where the patchy effects of extinction are also lowest. These facts together explain the relatively smooth appearance of the nucleus in the near-IR continuum.

NGC 7714 has been included in almost all samples of nuclear starburst galaxies, and is considered the archetypal UV-bright case. Taken as a whole, NGC 7714 lies on the relation between far-IR luminosity and UV continuum slope found by Meurer et al. (1999) for a sample of large aperture observations of UV-detected starbursts. Our analysis has shown that the central ~ 330 pc lie off this correlation, because of a few lines of sight with little obscuration towards hot stars. Most of the stars in this small aperture and in larger ones are more severely obscured. The global properties of NGC 7714, as probably those of many starburst galaxies, result from the averaging over many lines of sight with very diverse individual obscuration properties.

Incidentally, both M 82 and NGC 7714 have similar bolometric luminosities, indicating similar star-formation rates. What distinguishes the two galaxies is the dust column along the line of sight. M 82 is viewed almost edge-on, leading to a large dust column, and therefore large obscuration, whereas NGC 7714 is seen closer to pole-on, and the partially naked core is exposed. We can speculate that NGC 7714 would resemble M 82 if its inclination were similar.

What lessons have we learned from NGC 7714 for the derivation of star formation rates from the UV or the far-IR light? In agreement with Paper I, the analysis of the nuclear UV data alone indicates about $5 \times 10^6 M_{\odot}$ of ~ 5 Myr young stars. The total mass of stars of this most recent episode of star formation is most likely higher, by a factor of 2 to 4 (the Br γ emission carries the strongest evidence for the presence of obscured O,B stars, and the whole spectrum was necessary to set constraints on their number). The blue UV continuum of the nucleus of NGC 7714 is reproduced by the models as long as about 25 % of the hot stars is obscuration free. On a larger spatial scale, or in a more massive galaxy with a higher dust content, it becomes less likely that as much as 25 % of the young stars may happen to be obscuration free. The UV continuum will appear reddened, as it is the case for NGC 7714 in the IUE aperture and for most galaxies of the sample of Meurer et al. (1999). However, as most clearly demonstrated by Witt & Gordon (2000), the change in

UV slope only gives a lower limit to the actual attenuation of the UV light. IRAS galaxies with relatively blue UV continua confirm this bias (Meurer 2000).

While the UV light in NGC 7714 traces the most recent star formation to within a factor of a few, it clearly is blind to the $\sim 10^8 M_{\odot}$ of stars that were born over the larger timespan of a few 10^8 yrs. Our models show that the latter (in particular the stars born $10^7 - 10^8$ yrs ago) contribute a large fraction of the far-IR emission of the area. Thus, estimates from UV or far-IR measurements provide star formation rates averaged over different timescales. Information about the total duration of the star formation episode is necessary to estimate the real importance of a starburst. Gordon et al. (2000) show that the far-IR to UV flux ratio is a safe indicator of the UV attenuation for simple stellar populations. But for composite populations such as those of real starbursts we confirm the author's warnings that even this method is hazardous.

Acknowledgments:

J.G. performed most of his work on this paper while holding a postdoctoral fellowship at Space Telescope Science Institute. The STScI is also thanked for its hospitality to A.L. for two visits that made efficient progress possible. C.L. wishes to thank Observatoire de Strasbourg (Université Louis Pasteur) for its kind hospitality and support when this paper was finalized. This work was supported by HST grant GO-06672.01-95A from the Space Telescope Science Institute, which is operated by the Association of Universities for Research in Astronomy, Inc., under NASA contract NAS5-26555.

REFERENCES

- Bertola, F., Bettoni, D., Danziger, J., Sadler, E., Sparke, L., & de Zeeuw, T. 1991, *ApJ*, 373, 369
- Black, J. H., & van Dishoeck, E. F. 1987, *ApJ*, 322, 412
- Calzetti, D., Kinney, A. L., & Storchi-Bergmann, T. 1994, *ApJ*, 429, 582
- Calzetti, D. 1997, *AJ*, 113, 162
- Calzetti, D., Armus, L., Bohlin, R. C., Kinney, A. L., Koornneef, J., & Storchi-Bergmann, T. 2000, *ApJ*, 533, 682
- Cerviño, M., Luridiana, V., & Castander, F. J. 2000, *A&A*, 360, L5
- Condon, J.J., Condon M.A., Gisler, G., & Puschell, J.J. 1982, *ApJ*, 252, 102
- Doyon, R., Joseph, R. D., & Wright, G. S. 1994, *ApJ*, 421, 101
- Fioc, M., & Rocca-Volmerange, B. 1997, *A&A*, 326, 950
- Frogel, J. A., Persson, S. E., Matthews, K., & Aaronson, M. 1978, *ApJ*, 220, 75

- Glass, I.S., & Moorwood, A.F.M. 1985, MNRAS, 214, 429
- Goldader, J. D., Joseph, R. D., Doyon, R., & Sanders, D. B. 1995, ApJ, 444, 97
- . 1997, ApJ, 474, 104
- González Delgado, R. M., García-Vargas, M. L., Goldader, J., Leitherer, C., & Pasquali, A. 1999, ApJ, 513, 707
- González Delgado, R. M., & Leitherer, C. 1999, ApJS, 125, 479
- González Delgado, R. M., Leitherer, C., & Heckman, T. M. 1999, ApJS, 125, 489
- González Delgado, R. M., Leitherer, C., Heckman, T. M., & Cerviño, M. 1997, ApJ, 483, 705
- González-Delgado, R. M., Pérez, E., Díaz, A. I., García-Vargas, M. L., Terlevich, E., & Vílchez, J. M. 1995, ApJ, 439, 604
- Gordon, K. D., Calzetti, D., & Witt, A. N. 1997, ApJ, 487, 625
- Gordon, K. D., Clayton, G. C., Witt, A. N., & Misselt, K. A. 2000, ApJ, 533, 236
- Groenewegen, M. A. T., & de Jong, T. 1993, A&A, 267, 410
- Heckman, T. M., Robert, C., Leitherer, C., Garnett, D. R., & van der Rydt, F. 1998, ApJ, 503, 646
- Helou, G. 1986, ApJ, 311, L33
- Ho, P. T. P., Beck, S. C., & Turner, J. L. 1990, ApJ, 349, 57
- Howarth, I. D., 1983, MNRAS, 203, 301
- Iben, I., Jr., & Renzini, A. 1983, ARA&A, 21, 271
- Kawara, K., Nishida, M., & Phillips, M. M. 1989, ApJ, 337, 230
- Kotilainen, J. K., Reunanen, J. Laine, S., & Ryder, S. D. 2000, A&A, in press
- Lançon, A. 1998, in Asymptotic Giant Branch Stars, ed. T. Le Bertre, A. Lèbre, & C. Waelkens, IAU Symp. 191, 579
- Lançon, A., & Mouhcine, M. 2000, in Massive Stellar Clusters, ed. A. Lançon & C. Boily, ASP Conf. Ser. 211, 34
- Lançon, A., Mouhcine, M., Fioc, M., & Silva, D. 1999, A&A, 344, L21
- Lançon, A., & Wood, P. R. 2000, A&AS, in press
- Langer, N., & Maeder, A., 1995, A&A, 295, 685

- Lawrence, A., Ward, M., Elvis, M., Fabbiano, G., Willner, S. P., Carleton, N. P., & Longmore, A. 1985, *ApJ*, 291, 117
- Leitherer, C. 2000, in *Building the Galaxies: From the Primordial Universe to the Present*, ed. F. Hammer, T. X. Thuan, V. Cayatte, B. Guiderdoni, & J. T. T. Van (Singapore: World Scientific), 71
- Leitherer, C., & Heckman, T. M. 1995, *ApJS*, 96, 9
- Leitherer, C., Schaerer, D., Goldader, J. D., González Delgado, R. M., Robert, C., Foo Kune, D., de Mello, D., Devost, D., & Heckman, T. M. 1999, *ApJS*, 123, 3
- Lejeune, T., Cuisinier, F., & Buser, R. 1997, *A&A*, 125, 229
- Mas-Hesse, J. M., & Kunth, D. 1999, *A&A*, 349, 765
- Mazzarella, J. M., Bothun, G. D., & Boroson, T. A. 1991, *AJ*, 101, 2034
- Meurer, G. R. 2000, in *Starbursts Near and Far, Ringberg Workshop* (Sept. 2000; to be published)
- Meurer, G. R., Heckman, T. M., & Calzetti, D. 1999, *ApJ*, 521, 64
- Moorwood, A. F. M., & Oliva, E. 1988, *A&A*, 203, 278
- O'Halloran, B., Metcalfe, L., Delaney, M., McBreen, B., Laureijs, R., Leech, K., Watson, D., & Hanlon, L. 2000, *A&A*, 360, 871
- Origlia, L., Goldader J. D., Leitherer, C., Schaerer, D., & Oliva, E. 1999, *ApJ*, 514, 96
- Origlia, L., & Oliva, E. 1992, *A&A*, 254, 466
- Persson, S.E., Aaronson, M., Cohen, J. G., Frogel, J. A., Matthews, K. 1983, *ApJ*, 266, 105
- Puxley, P. J., & Brand, P. W. J. L. 1994, *MNRAS*, 266, 431
- Schmitt, H. R., Kinney, A. L., Calzetti, D., & Storchi-Bergmann, T. 1997, *AJ*, 114, 592
- Silva, D. R., & Bothun, G. D. 1998, *AJ*, 116, 2793
- Smith, B. J., & Wallin, J. F., 1992, *ApJ*, 393, 544
- Smith, B. J., Struck, J., & Pogge, R. 1997, *ApJ*, 483, 754
- Stevens, I. R., & Strickland, D. K. 1998, *MNRAS*, 294, 523
- Taniguchi, Y., Kawara, K., Nishida, M., Tamura, S., & Nishida, M. T. 1988, *AJ*, 95, 1378
- Ulvestad, J. S., & Antonucci, R. R. J. 1994, *ApJ*, 424, 29

Weedman, D. W., Feldman, F. R., Balzano, V. A., Ramsey, L. W., Sramek, R. A., & Wu, C.-C.
1981, ApJ, 248, 105

Witt, A. N., & Gordon, K. D. 2000, ApJ, 528, 799

Witt, A. N., Thronson, H. A., Jr., & Capuano, J. M., Jr. 1992, ApJ, 393, 611

Fig. 1.— H-band image of NGC 7714 taken with the CASPIR camera. The field size is $1'$. Regions are labelled as in González-Delgado et al. (1995).

Fig. 2.— Mosaic of the whole galaxy in the F380W filter, through WFPC2. The scale is $0.1''/\text{pixel}$; North is up, East to the left. The bridge between NGC 7714 and its companion (barely detected) is visible.

Fig. 3.— Nuclear zone of NGC 7714 in the PC1 chip of WFPC2, in the F380W (upper left) and F606W (upper right) filters. The scale is $0.046''$ per pixel. North is up and East is to the left. We also show the ratio F606W/F380W (lower left), indicating that most of the clusters are bluer than their surroundings (light=blue, dark=red). In the lower right panel, we show an unsharp-masked image in F380W, which emphasizes the dark lanes in the nucleus. Note that the dark lanes are somewhat red in the color image, and that one of the lanes passes over the apparent geometric center of the nucleus.

Fig. 4.— IR spectrum in an aperture of 1×5 pixels.

Fig. 5.— IR spectrum of the nucleus itself ($1.2'' \times 2.4''$ aperture).

Fig. 6.— Line fluxes and equivalent widths as a function of position along the slit. The top panel shows the fluxes of the Br γ , He I, and H $_2$ 1–0 S(1) lines in individual spatial rows. The middle panel shows the equivalent widths in individual rows. In the top and middle panels, the rightmost points for the He and H $_2$ lines are the sums of the lines in rows 14 and 15 of the spectrum. The bottom panel shows the spatial profile of the continuum emission. The slit passes across the nucleus (peaking at row 24), H II region B in rows 14 and 15, and H II region A at approximately row 28.

Fig. 7.— Observed velocities of the IR emission lines as function of position along the slit, along with the rotation curve derived for the H α line. The rotation curve is given after González-Delgado et al. (1995) and Bertola et al. (1991) as: $v(r) = \frac{Ar}{(r^2 + C_0^2)^{p/2}}$, where $A = 231 \text{ km s}^{-1}$, $C_0 = 8.3''$, and $p = 1.35$, for a spherical potential model with pure circular motions. As in González-Delgado et al. (1995), corrections have been made for both the inclination (assumed to be 45°), and the difference between the slit position angle and the major axis (assumed to be 35°).

Fig. 8.— Evolution of the UV and near-IR integrated magnitudes and of the corresponding color with aperture size.

Fig. 9.— The near-IR spectrum of NGC 7714, compared, from bottom to top, with the spectrum of a red giant, a red supergiant, an oxygen-rich variable AGB star and a carbon-rich AGB star. The spectra have been normalized to the same flux at $2.2 \mu\text{m}$, then shifted for display purposes.

Fig. 10.— Illustrative fit of the nuclear energy distribution of NGC 7714 with a simple, homogeneous star formation history, but an inhomogeneous dust distribution. Here, star formation has occurred constantly for 1 Gyr; $E(B - V) = 0$ for some lines of sight, 0.45 for others. The models shown are computed with Pégase and have the spectral resolution of the stellar library of Lejeune et al.

(1997).

Fig. 11.— Schematic representation of the recent star formation rates for two-component models that reproduce the UV-V-NIR nuclear spectrum of NGC 7714 rather well (right) and marginally well (left). However, these models fail to satisfy constraints outside this wavelength range (see text).

Fig. 12.— Two possible scenarios for the star formation in the nucleus of NGC 7714 over the last few 100 Myr. The star formation rate has been globally decreasing. The 5 Myr burst currently seen in the UV is part of a larger star formation scheme.

Fig. 13.— Illustrative fit of the nuclear spectrum with 3 successive bursts of decreasing burst masses. Dashed: burst age = 5 Myr, intrinsic $E(B - V) = 0.03$, $M = 4 \times 10^6 M_{\odot}$ (with the assumed 1 – 80 M_{\odot} Salpeter IMF). Dotted: burst age = 20 Myr, intrinsic $E(B - V) = 0.3$, $M = 7 \times 10^7 M_{\odot}$. Dot-dashed: burst age = 500 Myr, intrinsic $E(B - V) = 0.15$, $M = 3 \times 10^8 M_{\odot}$. $3.5 \times 10^8 L_{\odot}$, $4 \times 10^9 L_{\odot}$, and $4 \times 10^8 L_{\odot}$ of the light emitted by these components are absorbed by dust, resulting in a total contribution of $4.8 \times 10^9 L_{\odot}$ to the IRAS emission of the galaxy.

Fig. 14.— Illustrative fit of the nuclear spectrum, maximizing the contribution of the underlying spiral galaxy population to the near-IR light and minimizing the age of the recent star formation episode. Dashed: as in Fig. 13, with a stellar mass of nearly $4 \times 10^6 M_{\odot}$. Dotted: spiral galaxy population whose star formation rate followed a Schmidt law for 10 Gyr ($\text{SFR} = 0.3 M_{\odot} \text{ yr}^{-1} \times$ available gas mass, closed box), thus having produced about $7 \times 10^8 M_{\odot}$ of stars (in the 1–80 M_{\odot} mass range); intrinsic $E(B - V) = 0.29$. Dot-dashed: intermediate age population (exponentially decreasing SFR with an e -folding time of 50 Myr and an age of 200 Myr, $E(B - V) = 0.2$), $M = 1 \times 10^8 M_{\odot}$. $3.3 \times 10^8 L_{\odot}$, $1.3 \times 10^9 L_{\odot}$, and $1.6 \times 10^9 L_{\odot}$ of the light emitted by these components are absorbed by dust, providing a total contribution of $3.2 \times 10^9 L_{\odot}$ to the IRAS emission of the galaxy.

Fig. 15.— Correlation between global far-IR to UV flux ratios and the UV spectral index β . The stars and the dashed line are the data and the suggested relation of Meurer et al. (1999; their Fig. 1) for their sample of galaxies of various types. The square identifies NGC 7714 as observed through a large aperture. The rectangle shows the location of the nuclear region of NGC 7714 studied in this paper.

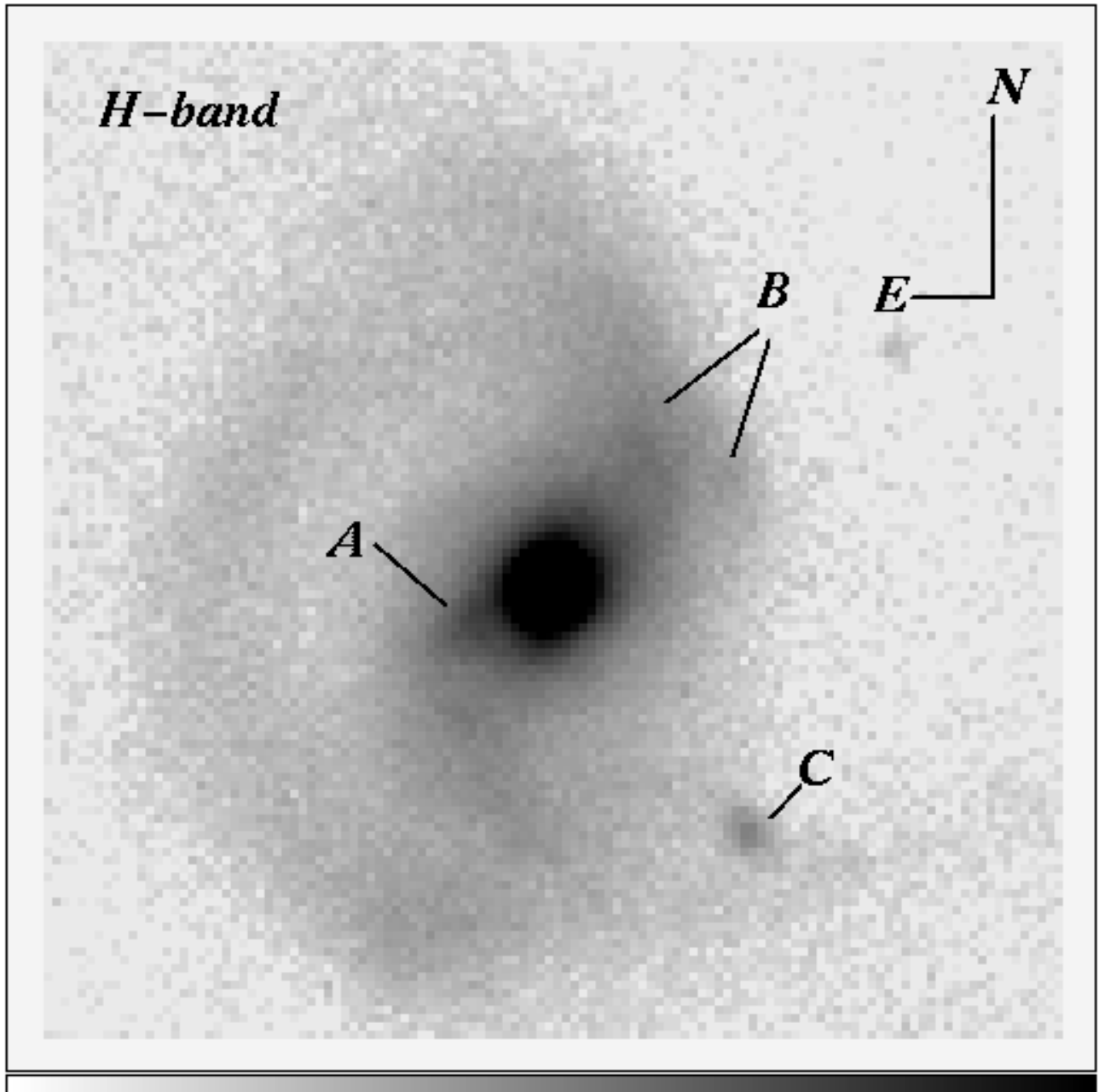


Fig. 1

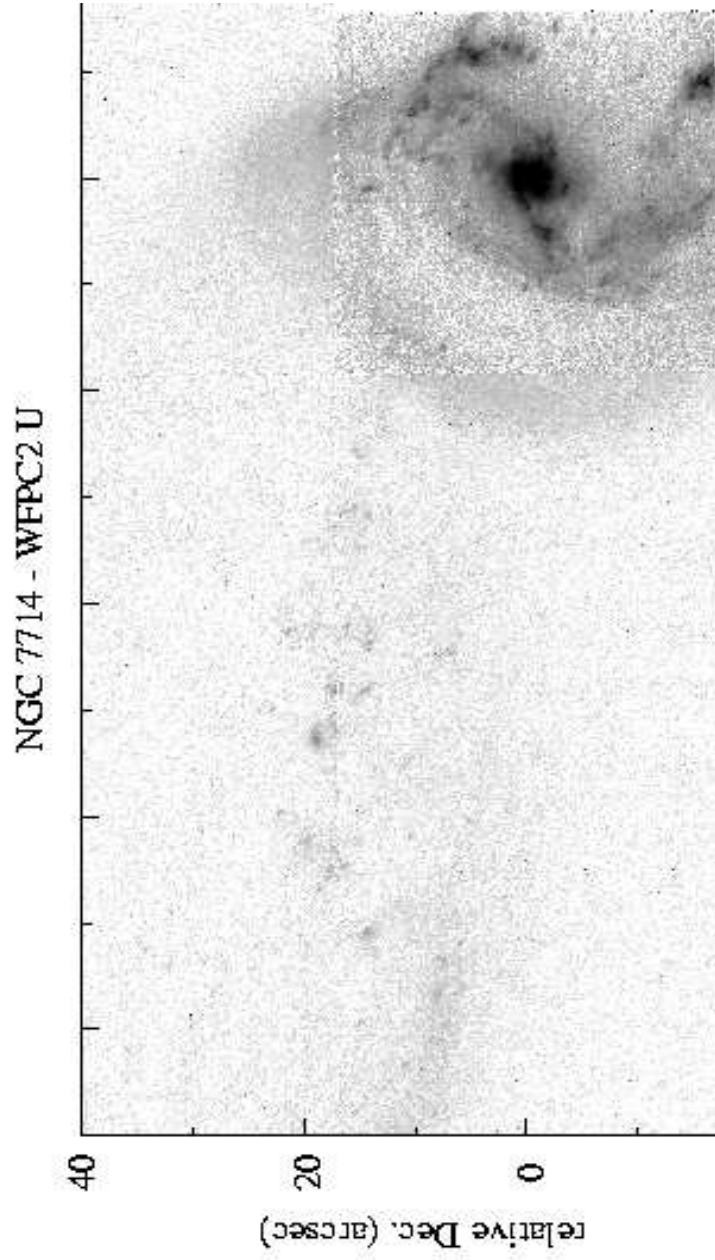


Fig. 2

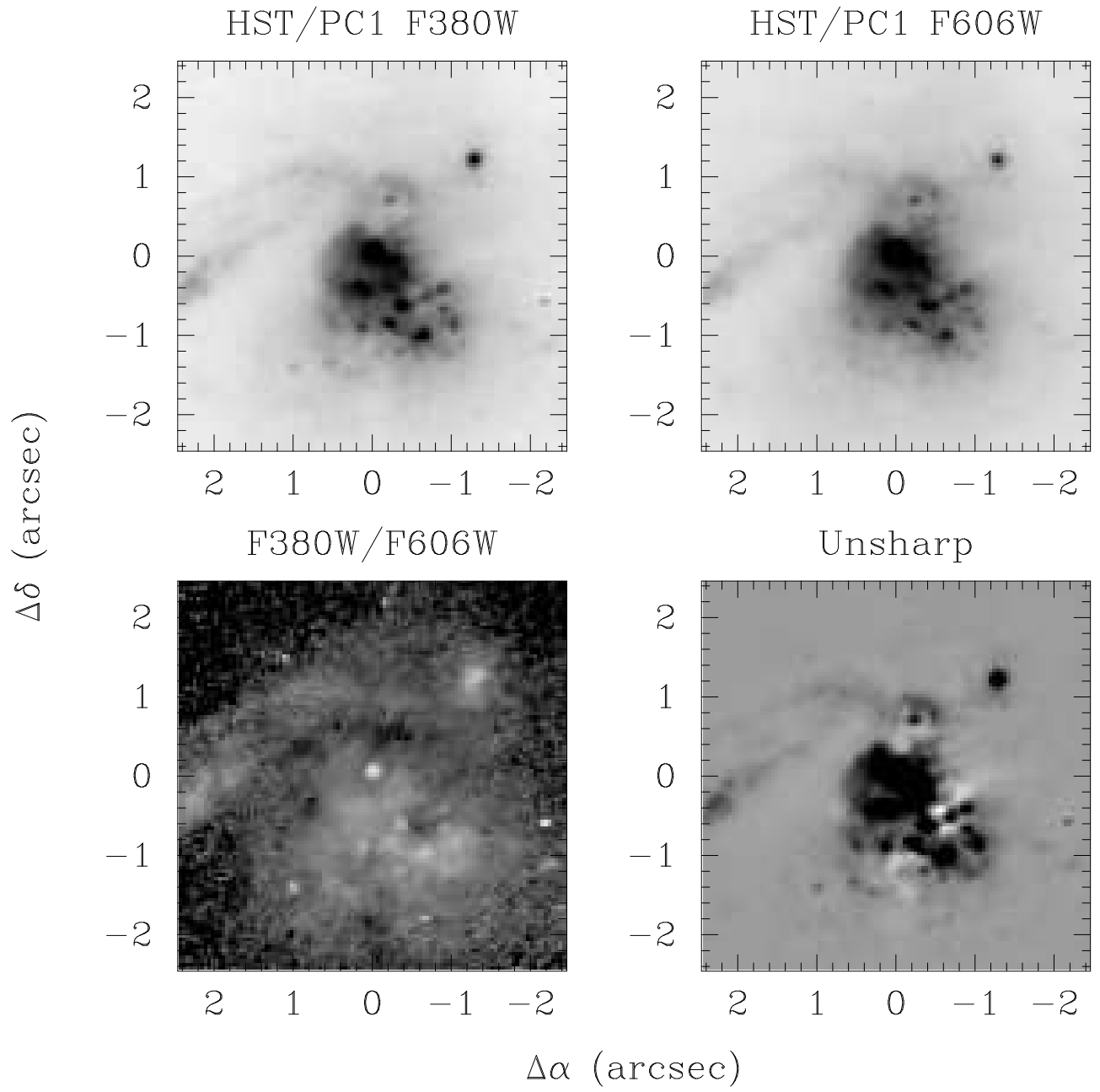


Fig. 3

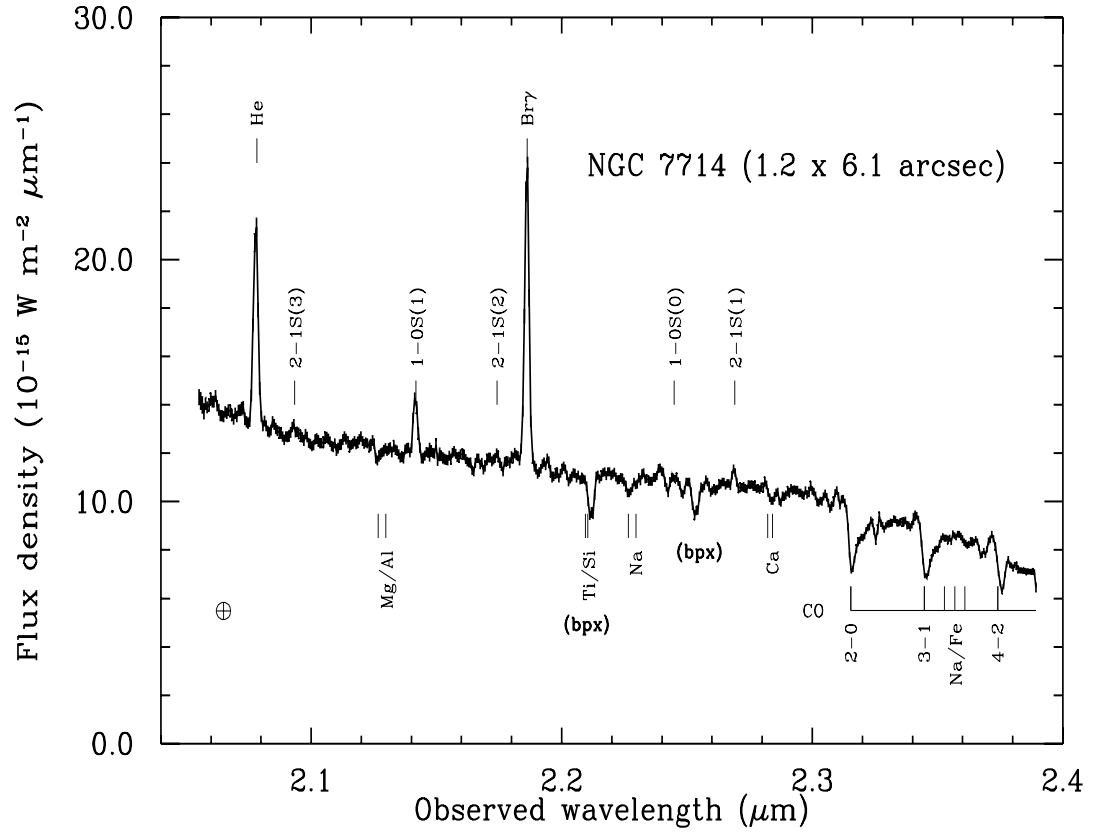


Fig. 4

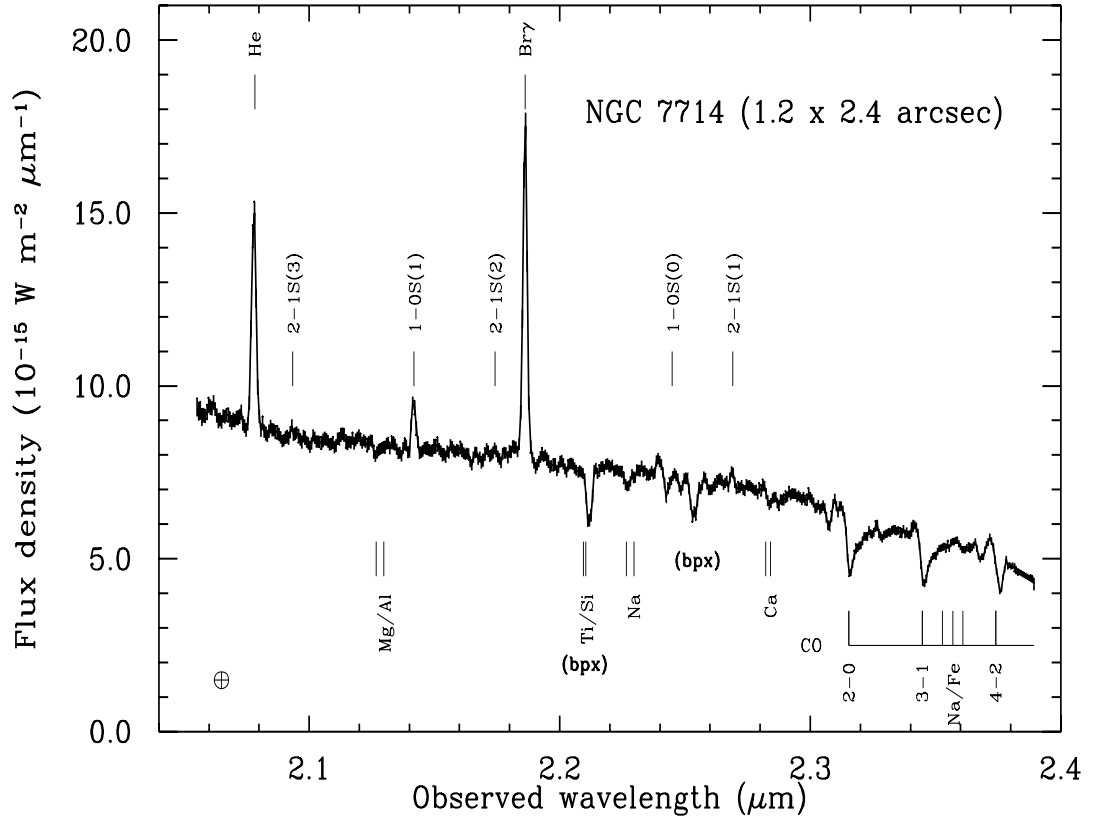


Fig. 5

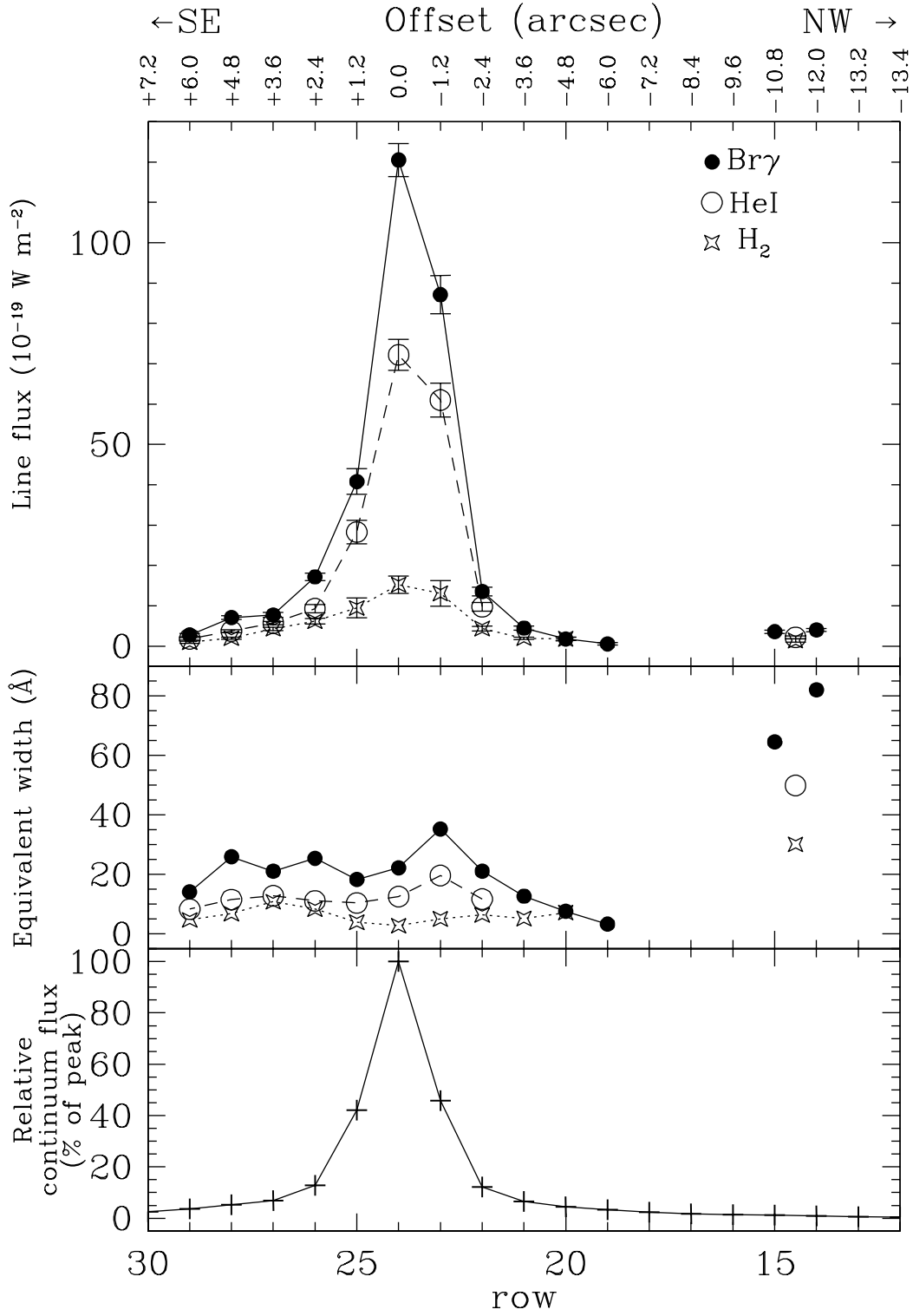


Fig. 6

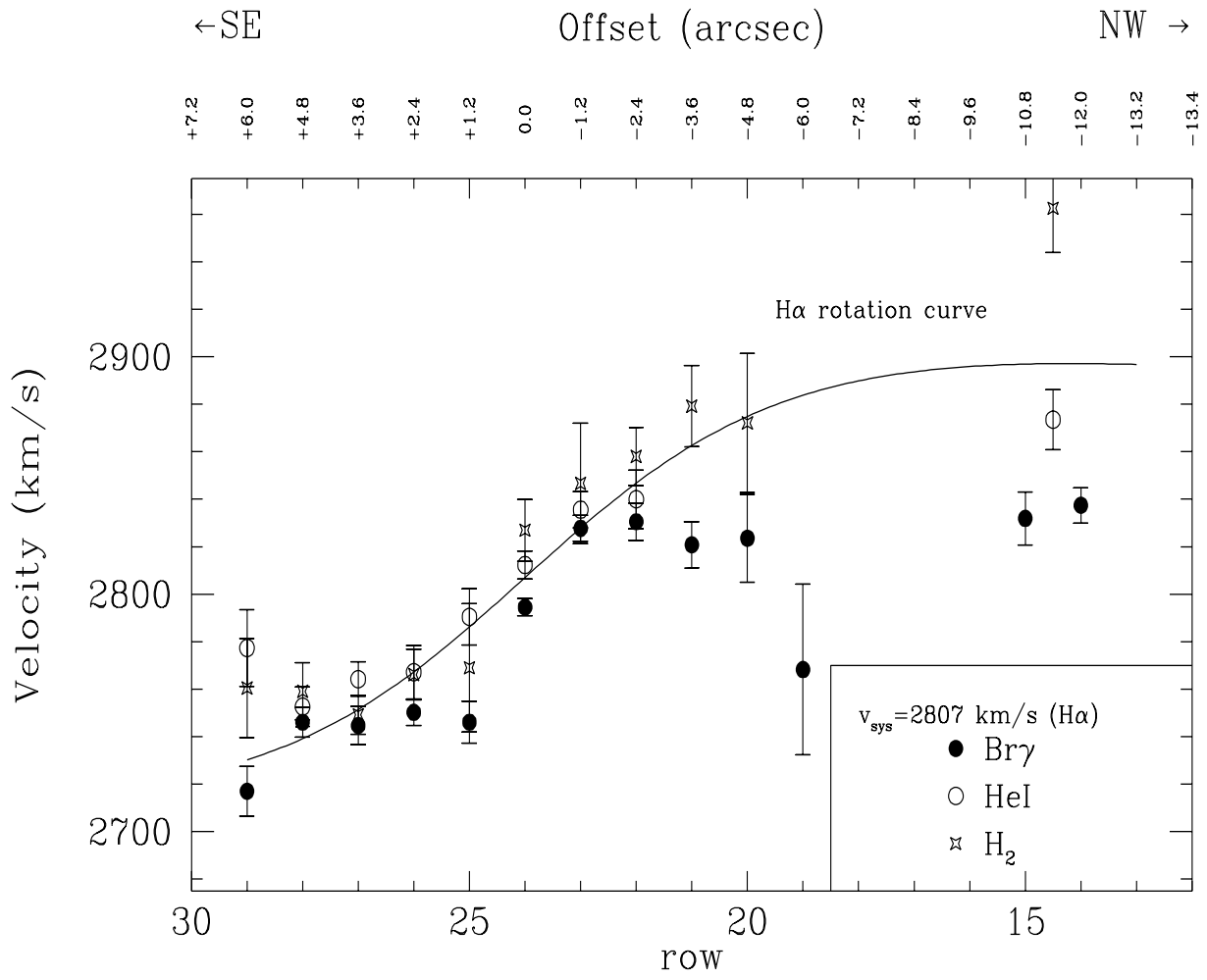


Fig. 7

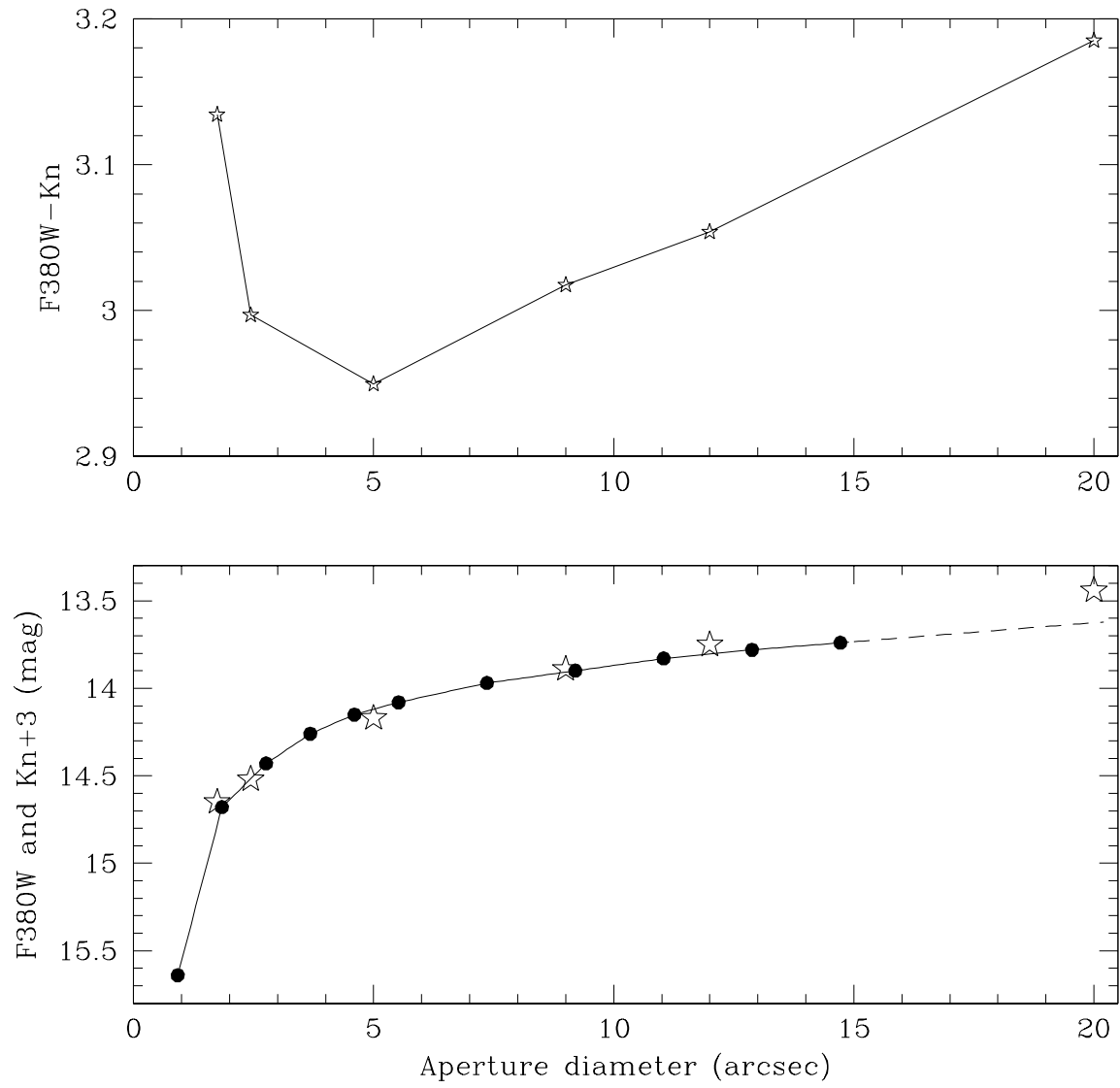


Fig. 8

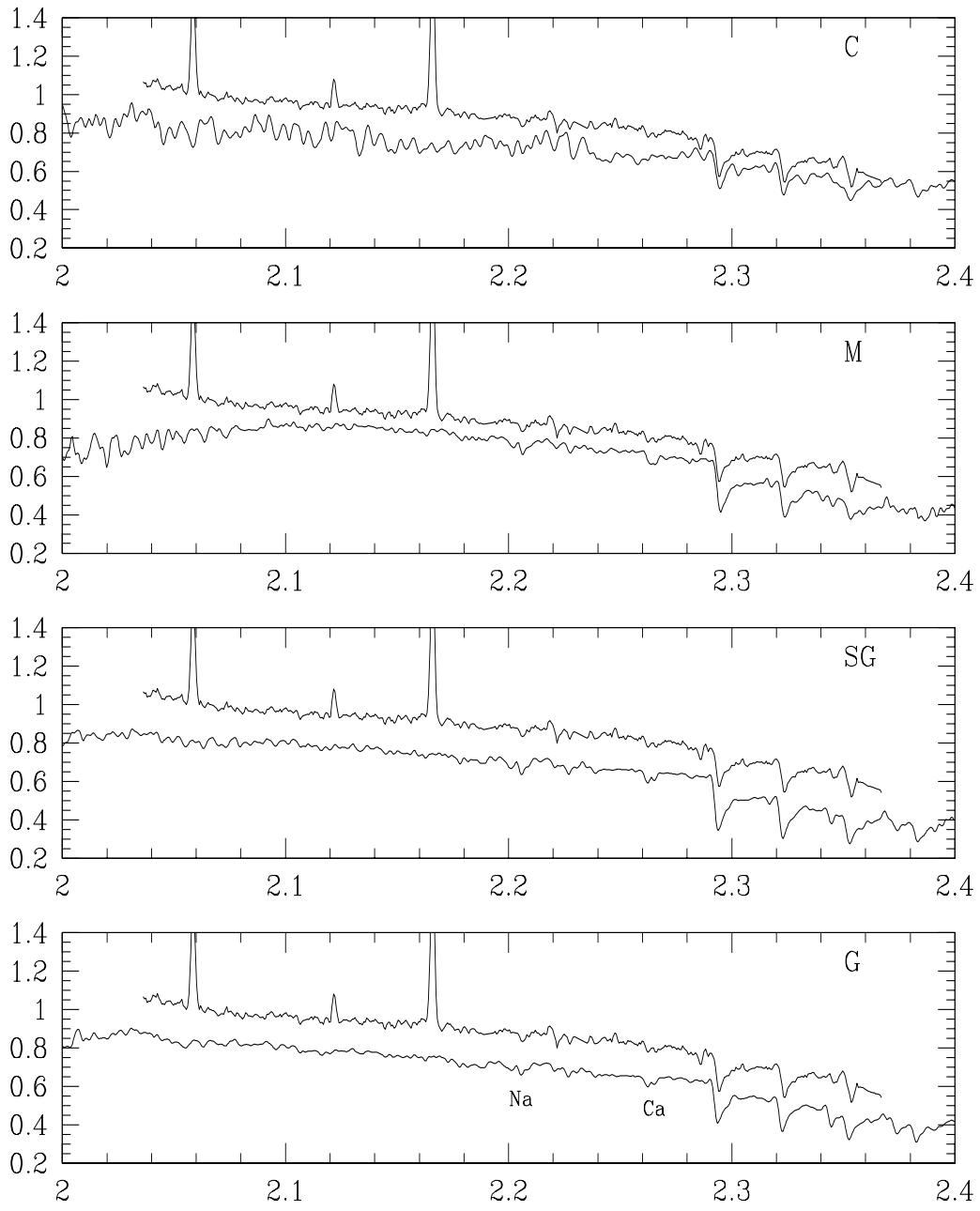


Fig. 9

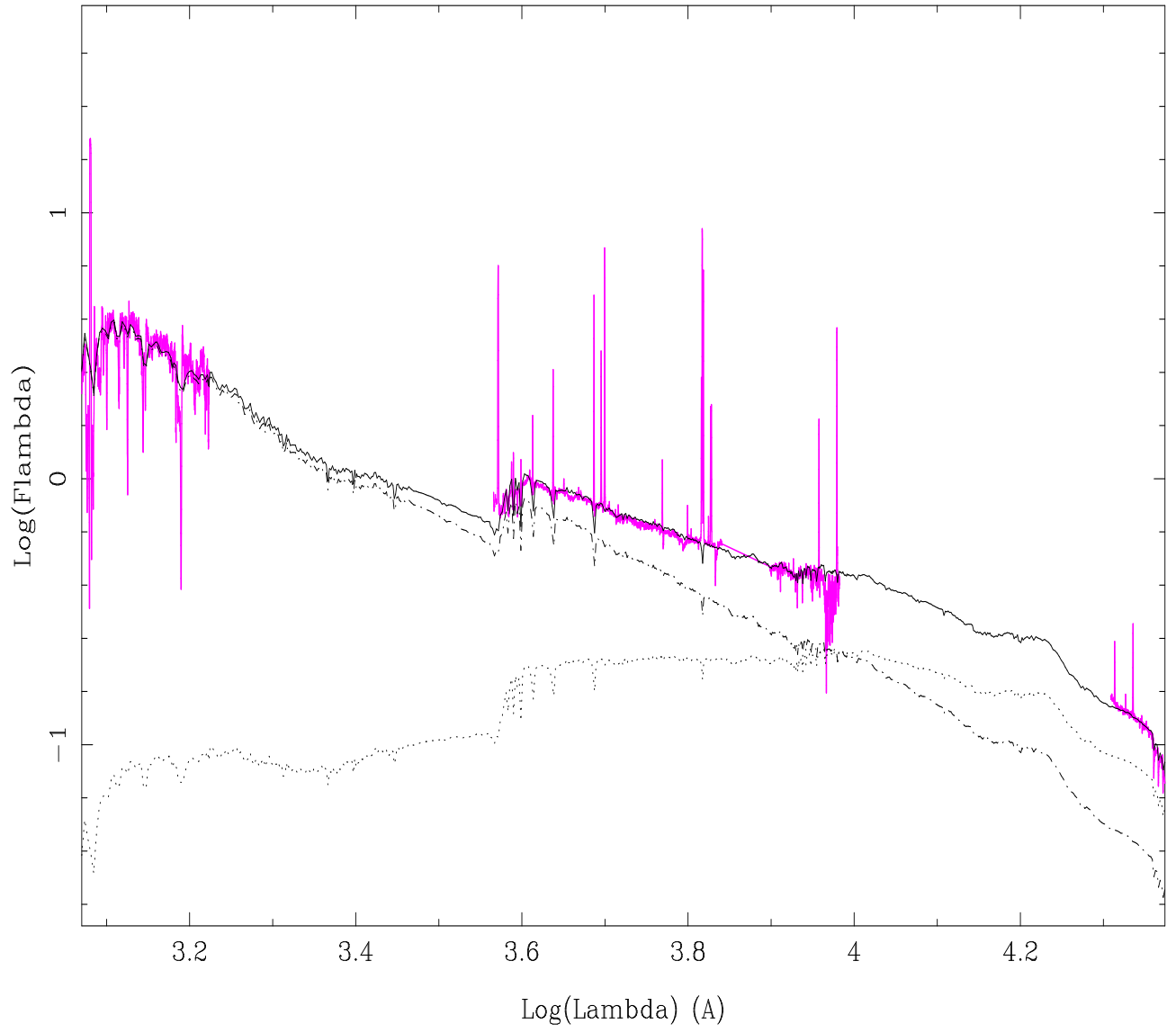


Fig. 10

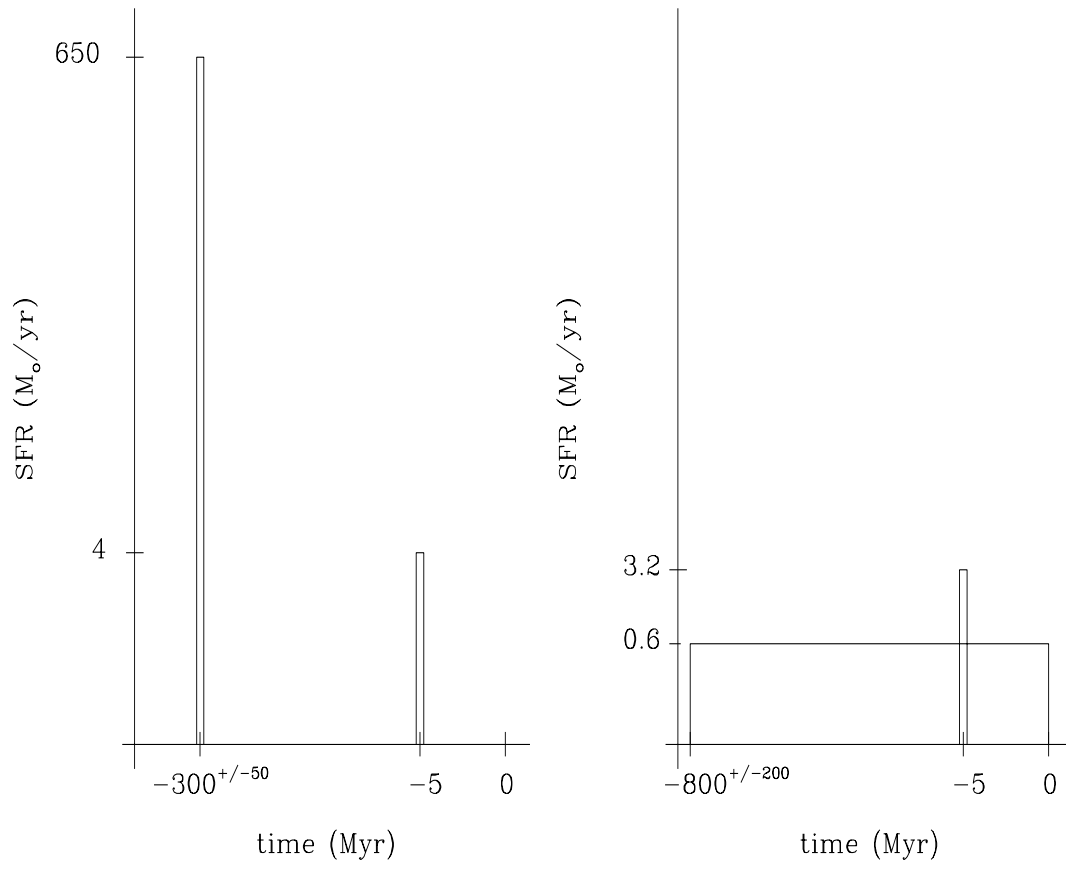


Fig. 11

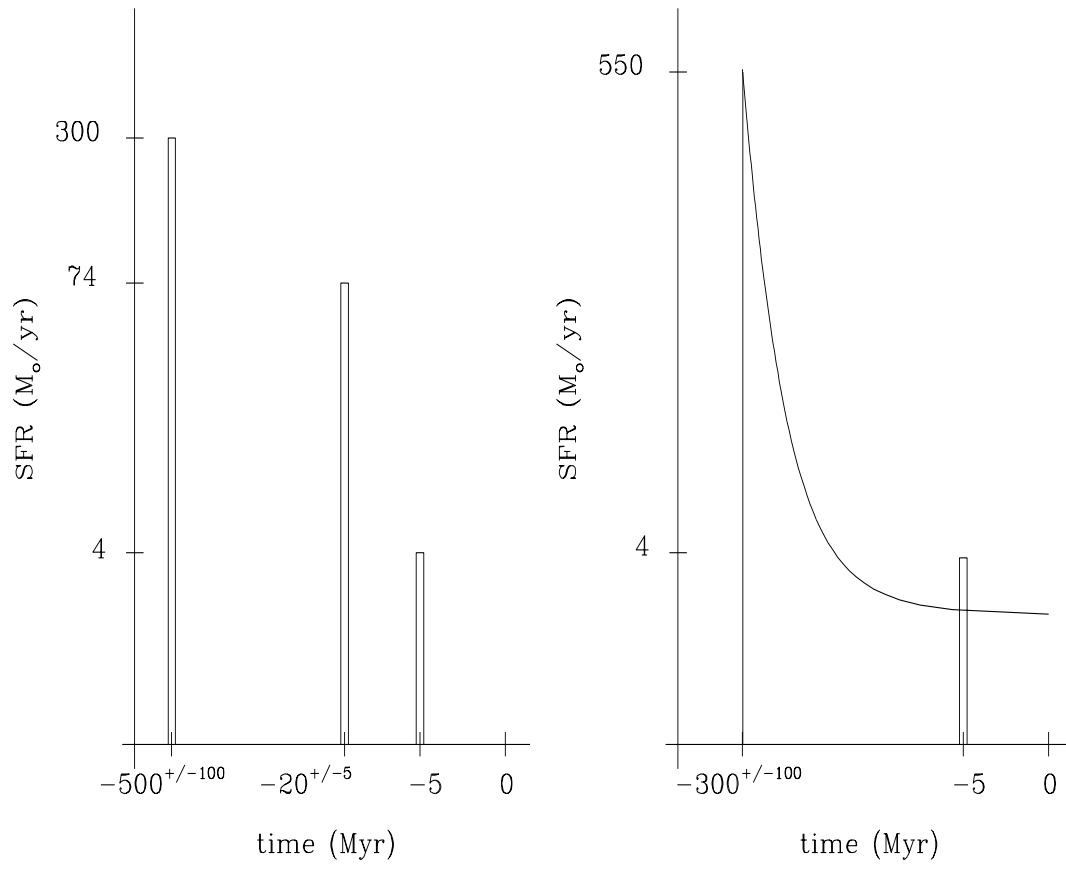


Fig. 12

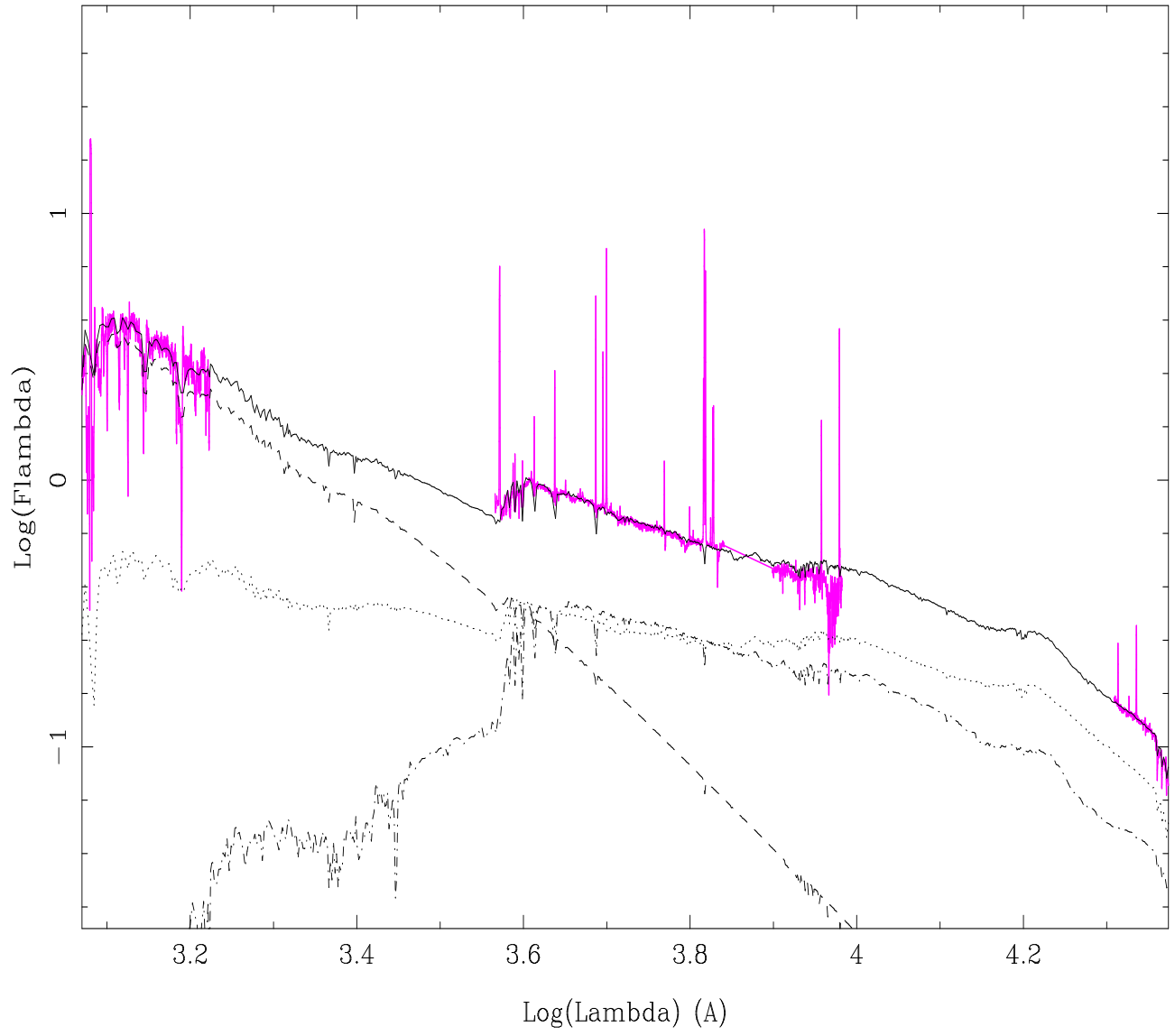


Fig. 13

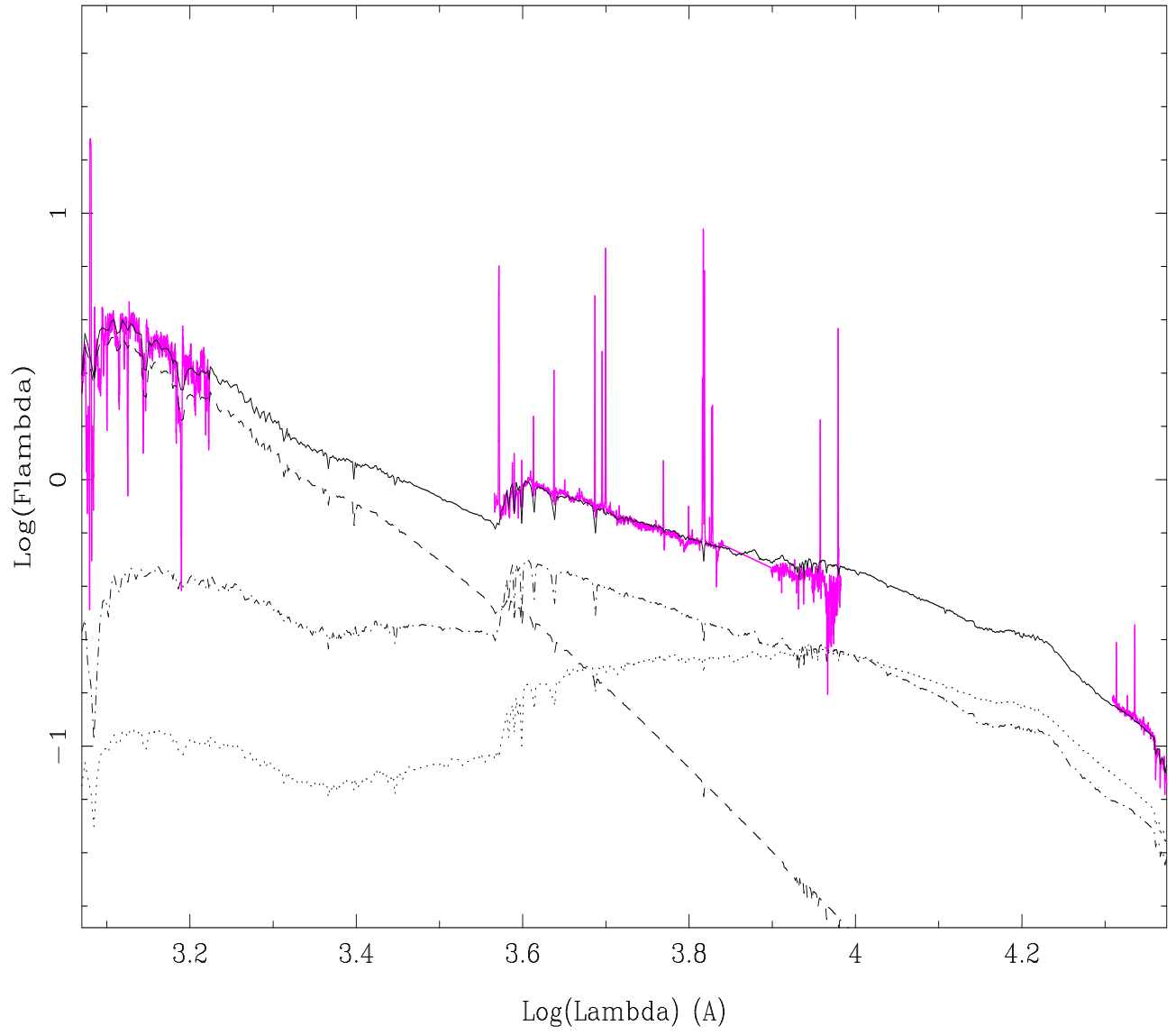


Fig. 14

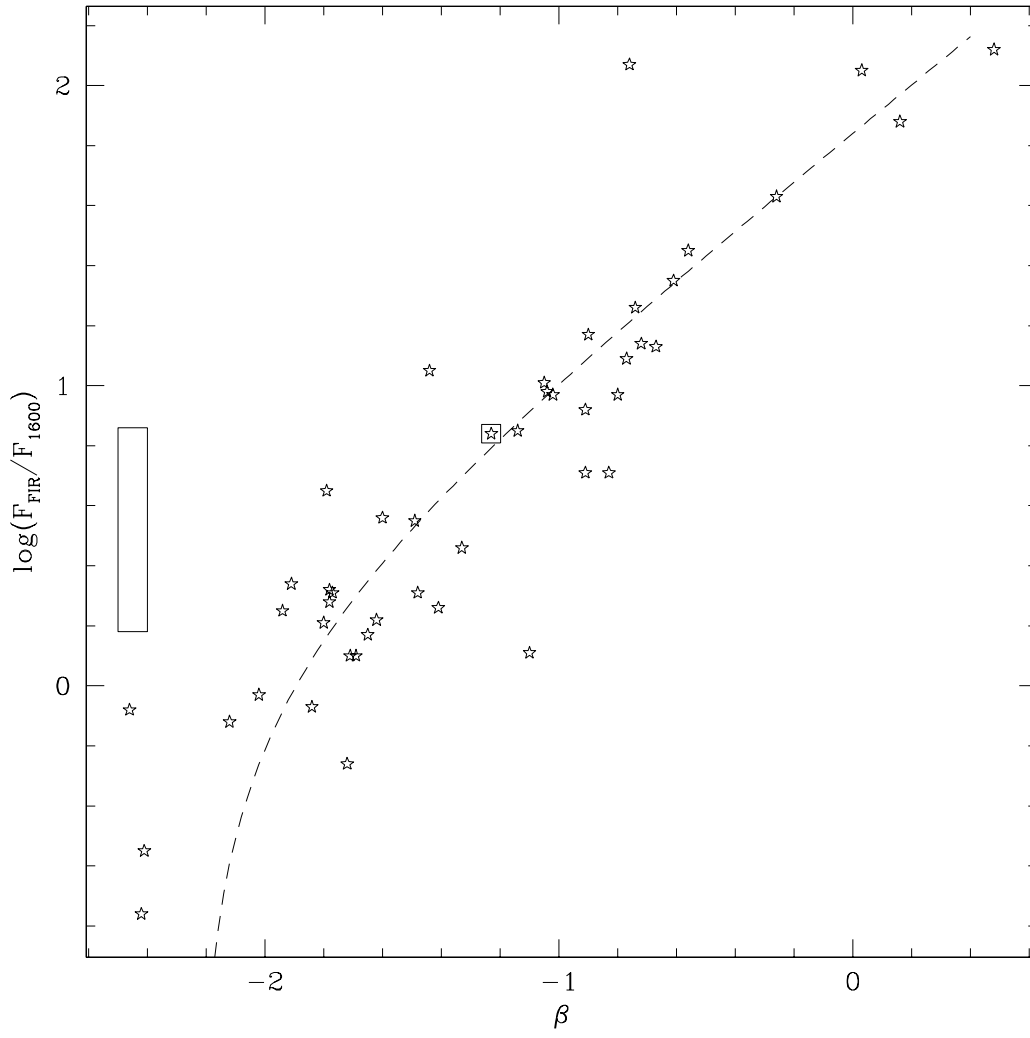


Fig. 15

Table 1: Near-IR Aperture Photometry of NGC 7714

Aperture diameter	This study			Literature			Reference
	<i>J</i> (mag)	<i>H</i> (mag)	<i>Kn</i> (mag)	<i>J</i> (mag)	<i>H</i> (mag)	<i>K</i> (mag)	
1.74''	12.66	11.99	11.65	
2.44''	12.51	11.85	11.52	
5''	12.13	11.47	11.17	12.27	11.56	11.23	<i>a</i>
9''	11.82	11.12	10.89	11.97	11.21	10.89	<i>b</i>
12''	11.72	11.02	10.75	11.81	11.08	10.77	<i>b</i>
20''	11.39	10.71	10.44	
34''	11.18	10.49	10.25	11.16	10.41	10.10	<i>b</i>

a- Lawrence et al. (1985); *b*- Glass & Moorwood (1985).

Table 2: F380W Aperture Photometry of NGC 7714

Radius	Magnitude
0.46''	15.64
0.92''	14.68
1.38''	14.43
1.84''	14.26
2.30''	14.15
2.76''	14.08
3.68''	13.97
4.60''	13.90
5.52''	13.83
6.44''	13.78
7.36''	13.74

Table 3: Selected K-band Line Fluxes in NGC 7714

Line	Flux ^a (10 ⁻¹⁹ W m ⁻²)
(1)	(2)
Aperture 1.22'' × 6.10'' (Central)	
HeI	191.0 ± 6.8
H ₂ 2–1 S(3)	< 17.2 (3σ)
H ₂ 1–0 S(1)	40.9 ± 4.3
H ₂ 2–1 S(2)	< 16.0 (3σ)
Brγ	274.5 ± 7.4
H ₂ 1–0 S(0)	< 13.8 (3σ)
H ₂ 2–1 S(1)	18.1 ± 4.0
Aperture 1.22'' × 2.44'' (Nuclear)	
HeI	139.0 ± 5.8
H ₂ 2–1 S(3)	< 14.4 (3σ)
H ₂ 1–0 S(1)	27.2 ± 3.7
H ₂ 2–1 S(2)	< 13.6 (3σ)
Brγ	209.6 ± 6.2
H ₂ 1–0 S(0)	< 11.4 (3σ)
H ₂ 2–1 S(1)	8.4 ± 3.1
Two outer pixels	
HeI	18.6 ± 1.5
H ₂ 2–1 S(3)	< 4.3 (3σ)
H ₂ 1–0 S(1)	10.6 ± 1.0
H ₂ 2–1 S(2)	< 3.4 (3σ)
Brγ	29.4 ± 1.4
H ₂ 1–0 S(0)	5.3 ± 0.9
H ₂ 2–1 S(1)	3.1 ± 0.9

a. The quoted errors are from the fitting procedure and do not include the estimated 10% calibration uncertainty.

Table 4: H₂ Line Ratios in NGC 7714

Aperture (1)	Ratio			
	$\frac{2-1S(3)}{1-0S(1)}$ (2)	$\frac{2-1S(2)}{1-0S(1)}$ (3)	$\frac{1-0S(0)}{1-0S(1)}$ (4)	$\frac{2-1S(0)}{1-0S(1)}$ (5)
“Central” spectrum (1.2'' × 6.1'')	< 0.42	< 0.39	< 0.34	0.44 ± 0.11
“Nuclear” spectrum (1.2'' × 2.4'')	< 0.53	< 0.50	< 0.42	0.31 ± 0.12
Two outer pixels	< 0.41	< 0.32	0.50 ± 0.10	0.29 ± 0.09
Black & van Dishoeck model 14	0.35	0.28	0.46	0.56
Black & van Dishoeck model S2	0.08	0.03	0.21	0.08

Table 5: Br γ Fluxes in NGC 7714

Aperture	Flux ($10^{-18} \text{ W m}^{-2}$)	Source ^a
(1)	(2)	(3)
1.22'' \times 2.44''	21.0 \pm 0.6	<i>a</i>
1.22'' \times 6.10''	27.5 \pm 0.7	<i>a</i>
3.5'' \times 7''	26.4 \pm 3.8	<i>b</i>
3.1'' \times 9.3''	29.5 \pm 2.2	<i>c</i>
6'' \times 6''	30 \pm 3	<i>d</i>
7'' diam.	47 \pm 5	<i>e</i>
10'' \times 20''	49.9 \pm 2.0	<i>f</i>
10.3'' \times 20.7''	51 \pm 12	<i>g</i>

a- This paper; *b*- Taniguchi et al. (1988); *c*- Puxley & Brand (1994); *d*- Moorwood & Oliva (1988);
e- Ho et al. (1990); *f*- Calzetti (1997); *g*- Kawara et al. (1989).